Spring 2010

Predictions of saturated hydraulic conductivity dynamics in a midwestern agricultural watershed, Iowa

Yi-Jia Chang
University of Iowa

PREDICTIONS OF SATURATED HYDRAULIC CONDUCTIVITY DYNAMICS IN A MIDWESTERN AGRICULTURAL WATERSHED, IOWA

by

Yi-Jia Chang

A thesis submitted in partial fulfillment
of the requirements for the
Master of Science degree in
Civil and Environmental Engineering
in the Graduate College of
The University of Iowa

May 2010

Thesis Supervisor: Professor Athanasios N. Papanicolaou

Graduate College
The University of Iowa
Iowa City, Iowa

CERTIFICATE OF APPROVAL

MASTER'S THESIS

This is to certify that the Master's thesis of

Yi-Jia Chang

has been approved by the Examining Committee for the thesis requirement for the Master of Science degree in Civil and Environmental Engineering at the May 2010 graduation.

Thesis Committee: _____
Athanasios N. Papanicolaou, Thesis Supervisor

_____
Nandita Basu

_____
Kathleen Stewart

And let the peace of God rule in your hearts, to the which also ye are called in one body; and be ye thankful.

Colossians 3:15

ACKNOWLEDGEMENTS

First and foremost, my deepest thankfulness is given to my God and Lord for all of the grace and blessings that I have received throughout my time in the United States. I thank my father, mother and family in Taiwan for their unlimited love and support in my life. I also would like to express my appreciation to my beloved Apostolic Christian Church families and brethren, especially the Rassis, Wagenbachs, Hartmans, Elands, Plattners, and Bazzells. Your care and love have been very encouraging for me to continue to overcome the difficult time of life.

This study was funded by the United States Department of Agriculture - Natural Resources Conservation Service (NRCS) National Soil Survey Center (NSSC). I would like to express my great appreciation and deep gratitude to my advisor, Prof. Thanos Papanicolaou for placing at my disposal all scientific means necessary for this research. I value his expertise, supportiveness, understanding, guidance and encouragement. I thank my thesis committee members, Nandita Basu and Kathleen Stewart, for their valuable time and enormous suggestions that helped this study be more complete. I would like also to thank Dr. Mohamed Elhakeem and Dr. Christopher Wilson for their supervision during the study.

I would like to thank Mike Sucik (State Soil Scientist, Iowa NRCS) for coordinating efforts with Ryan Dermody, Lee Camp and Neil Sass (soil Scientists at Waverly Soils Office; NRCS - Bremer County, IA), who assisted in core collection. In addition, the cooperation of the local farmers in the South Amana area is also appreciated. I would like to thank Steve Johnston and James Martin (NRCS Iowa County) for working with us in identifying the farmer participants. Finally, I would like to thank the IIHR staff who assisted in the field work including the following: Fabienne Bertrand, Kevin Denn, Dimitrios Dermisis, Ken Wacha, Philip Ellis, Achilles Tsakiris, and Timothy Lauth.

ABSTRACT

In this study, a physically-based, modeling framework was developed to predict saturated hydraulic conductivity (K_{sat}) dynamics in the Clear Creek Watershed (CCW), IA. The modeling framework integrated selected pedotransfer functions (PTFs) and watershed models with geospatial tools. A number of PTFs and watershed models were examined to select the appropriate models that represent the study site conditions. Models selection was based on statistical measures of the models' errors compared to the K_{sat} field measurements conducted in CCW under different soil, climatic and land use conditions. The study has shown that combined Rosetta and the Water Erosion Prediction Project (WEPP) predictions provided the best agreement to the measured K_{sat} values in the CCW compared to the other tested models. Therefore, Rosetta and WEPP were integrated with the Geographic Information System (GIS) tools by developing a program for data registries. The modeling framework allowed for visualization of the data in forms of geospatial maps and prediction of K_{sat} variability in CCW due to the seasonal changes in climate and land use activities.

Two seasons were selected to demonstrate K_{sat} dynamics; specifically, the months of October and April, which corresponded to the before harvesting and before planting conditions, respectively. Baseline saturated hydraulic conductivity (K_b) exhibited higher values on the northern part of the CCW compared to the southern part due to differences in soil texture. For bare saturated hydraulic conductivity (K_{br}), the month of April had overall higher values than the month of October, because K_{br} is inversely proportional to cumulative rainfall kinetic energy and spring season in Iowa are characterized by lower precipitation compared to the fall season.

Except for the ungrazed grassland areas, effective K_{sat} that accounts for land cover only ($K_{e\text{-}nr}$) did not change significantly with season, exhibiting the lowest values at the forest and urbanized areas in the CCW. The corn fields showed lower $K_{e\text{-}nr}$ values than

soybean fields due to different characteristics of the crops. The effects of rainfall on effective saturated hydraulic conductivity (K_e) were demonstrated by the single storm events of October 17th, 2007 and April 18th, 2008. The former showed higher K_e in CCW, because K_e is linearly proportional to rainfall depth and the October event had higher precipitation than the April event.

Statistical analysis of the K_{sat} data in CCW has shown that the geometric mean or median was more representative for the distributions of different expressions of saturated hydraulic conductivities due to their wide ranges. The values of K_b were the highest values among the other expressions of K_{sat}. $K_{e\text{-}nr}$ values were smaller than K_b values, while K_e values were higher than $K_{e\text{-}nr}$.

The applicability of the pedotransfer functions and watershed models used within the developed modeling framework is limited to the investigated watershed and other watersheds in Iowa having similar soils, management practices, and climatic conditions, mostly in the semihumid region of eastern Iowa. As the proposed modeling framework was able to successfully capture the spatial and temporal variability of K_{sat} at the watershed scale, it would be advisable to repeat this study in different counties or even in other parts of the country, where arid or semi-arid conditions are ubiquitous, using different pedotransfer functions and watershed models. This can contribute to the development of ratings for many of the soil interpretations incorporated into the National Cooperative Soil Survey (NCSS) and update the K_{sat} data stored in the National Soil Information System (NASIS) database.

TABLE OF CONTENTS

LIST OF TABLES

LIST OF FIGURES

LIST OF SYMBOLS

English Symbols

BD	$g \cdot cm^{-3}$	Bulk density
C	m^2/J	Soil stability factor
C_C	fraction	Canopy cover
C_{CE}	fraction	Effective canopy cover
C_{CF}	dimensionless	Correction factor of effective canopy cover
CEC	meq/100g	Cation exchange capacity
CF	dimensionless	Crust factor
Cf	m^2/kg	Crop specific constant that is specified by the type of crops
Cl	fraction	Clay content
C_R	fraction	Residue cover
C_{RF}	fraction	Flat residue cover
C_{RS}	fraction	Standing residue cover
C_{RT}	fraction	Total residue cover
C_{TE}	fraction	Total effective surface cover
E_a	J/m^2	Cumulative rainfall kinetic energy since the last tillage
E_R	$J/m^2 \cdot h$	Rainfall kinetic energy
H	m	Fall height or canopy height
I	mm/h	Rainfall intensity
K_{sat}	mm/h	Saturated hydraulic conductivity
K_b	mm/h	Baseline saturated hydraulic conductivity considering the effects of soil textures and bulk density
K_{br}	mm/h	Bare saturated hydraulic conductivity considering the factors of crusting, tillage and cumulative rainfall kinetic energy
K_e	mm/h	Effective saturated hydraulic conductivity considering K_b, K_{br}, single storm precipitation, land cover
L	m	Wetting front depth
m		Median
M_f	kg/m^2	Flat residue biomass
P	mm	Storm rainfall amount
p	ratio	Porosity
RR_t	m	Random roughness
Sa	fraction	Sand content
SC	dimensionless	Correction factor for partial saturation of the sub-crust soil
Si	fraction	Silt content
T_R	hour	Total rain time
X_i		Data points
X_j		Data points

Greek Symbols

α	dimensionless	Parameter of the type of rain
β	dimensionless	Parameter of the type of rain
μ_a		Arithmetic mean
μ_g		Geometric mean
μ_h		Harmonic mean
σ_a		Arithmetic standard deviation
σ_g		Geometric standard deviation
Ψ	dimensionless	Steady state capillary potential at the crust/sub-crust interface
Φ		Function

CHAPTER 1 INTRODUCTION

Infiltration, the entry of water from rainfall, snowmelt, or irrigation, into the soil is an integral component of the Earth's hydrologic cycle (e.g., Linsley et al. 1982, McCuen 2003). The rate of infiltration is mainly controlled by soil texture, antecedent moisture condition, rainfall intensity/duration, landscape, land use and associated management practices (e.g., McCuen 2003, Ben-Hur and Wakindiki 2004, Elhakeem and Papanicolaou 2009). When the infiltration rate reaches a steady state condition, it is defined in the literature as the saturated hydraulic conductivity, also known as K_{sat} (e.g., Zaslansky and Sinai 1981, Potter 1990, Rawls et al. 1990, Nearing et al. 1996, McCuen 2003).

K_{sat} is a key variable in hydropedologic studies determining soil suitability for agricultural uses, water relationships for plant growth, and potentials for pesticide leaching (Tugel et al. 2007, West et al. 2008). In addition, K_{sat} directly influences the amount of runoff and eroded surface soil that are delivered to local waterways, thereby affecting both in-field soil quality and in-stream water quality (Elhakeem and Papanicolaou 2009, Abaci and Papanicolaou 2009). K_{sat} is also used to develop ratings for many soil interpretations incorporated into the National Cooperative Soil Survey (NCSS), and is one of the key input variables for the majority of the physically-based watershed models used for the assessment of the impacts of the land uses and management practices on the dynamic behavior of soil and water [e.g., WEPP (Nearing et al. 1996); SWAT (Arnold et al. 1998)]. Therefore, accurate estimate of K_{sat} and its statistical properties is of paramount importance for predicting hydrologically-driven processes and making catena assessments in landscapes (e.g., Nearing et al. 1996, Lin 2003, Schoeneberger and Wysocki 2005, Nordt et al. 2006, Jarvis 2007, Papanicolaou and Abaci 2008).

1.1 Problem Statement

K_{sat} exhibits large spatial and temporal variability at both large and small scales due to various combinations of the intrinsic soil properties (e.g., texture, bulk density) and extrinsic factors such as land use, canopy cover, and precipitation (e.g., Tietje and Richter 1992, Webster and Oliver 2001, West et al. 2008, Papanicolaou et al. 2008a). Spatial variability of K_{sat} due to regional differences is controlled by intrinsic soil properties, whereas the added seasonal variability of K_{sat} within a region is due to the extrinsic factors. Most of the K_{sat} values reported in the databases (e.g., NCSS, UNSODA, WISE, HYPRES) are based on intrinsic soil properties, which limits, in many instances, the direct use of these data without correction for the extrinsic factors (e.g. Carsel and Parrish 1988, Leij et al. 1996, Batjes 1996, Wosten et al. 1999). While spatial variability of K_{sat} at a specific site can be captured only via detailed field measurements, temporal variability at this site requires continuous measurements over long periods (Papanicolaou et al. 2009).

Direct measurements of K_{sat} at a specific site via standard instruments such as the Double Ring Infiltrometer (DRI), the Rainfall Simulator (RS), or the Amoozemeter (AM) provide the most representative values for K_{sat}. However, in-situ measurements of K_{sat} are often expensive, labor-intensive and typically have a sparse spatial resolution. Due to these limitations, field investigations often result in an incorrect portrayal of causal linkages and long-term trends (e.g., Smith 2002). Automation of the instruments has partially addressed the concerns associated with the intensive workload during field surveys (e.g., Papanicolaou et al. 2008a, Papanicolaou et al. 2009, Elhakeem and Papanicolaou 2009). Yet, a significant number of measurements are still needed to adequately quantify K_{sat} variability at the hillslope scale (10^3-10^5 m^2). Also, the performance of continuous, spatial distributed measurements, even with the automated instruments, remains a challenging task.

For hydropedologic studies at scales larger than the hillslope (i.e., watershed, township, county, state, etc.), rapid but robust methods for K_{sat} prediction are still needed, where in-situ measurements may not be feasible. Indirect methods for K_{sat} prediction, which involve, for example, infiltration models coupled with geospatial tools can potentially address the spatial and dynamic limitations related to the field methods. However, indirect methods need to be complemented with field data for calibration and verification.

1.2 Objectives

The main objective of the proposed research study is to introduce an integrative modeling method to make adequate predictions of K_{sat} under different intrinsic and extrinsic factors and at scales where management and policy decisions must be made (e.g., watershed, township, county, state, etc.). A geospatial-physically based, modeling framework, within which geographic, climatic, and land uses data can be incorporated, has been developed. The model integrates watershed models and pedotransfer functions (PTFs) with geospatial-tools to predict K_{sat} as a function of some intrinsic soil properties and extrinsic factors. The ultimate goal of this research is to utilize the proposed modeling framework in the Clear Creek Watershed (CCW), IA by adapting it to site-specific parameters. The model would predict K_{sat} dynamics in the CCW due to the seasonal changes in climate and land use activities. The study incorporates also selective field measurements for model calibration.

CHAPTER 2 LITERATURE REVIEW

K_{sat} is a function of both intrinsic soil properties, such as texture, bulk density, organic matter, and extrinsic factors, such as vegetation, land use, management practices, and precipitation (e.g., Onstad et al. 1984, Mohanty et al. 1994, Govindaraju et al. 1995, Gupta et al. 1996, Rahman et al. 1996, Diiwu et al. 1998, West et al. 2008, Wosten et al. 1999, Papanicolaou et al. 2008b). Spatial variability of K_{sat} due to regional differences is controlled by intrinsic soil properties, while the added seasonal variability of K_{sat} within a region is due to the extrinsic factors (e.g. Carsel and Parrish 1988, Leij et al. 1996, Batjes 1996, Wosten et al. 1999). In the literature, K_{sat} that accounts for only intrinsic soil properties is referred to as the baseline hydraulic conductivity, K_b, whereas K_{sat} that incorporates the extrinsic factors, in addition to the soil properties, is defined as the effective hydraulic conductivity, K_e (Potter 1990, Nearing et al. 1996, Schoeneberger and Wysocki 2005).

Numerous field methods and infiltration models have been established for estimating K_{sat}. The following sections describe some of these methods and models:

2.1 Field Methods

Many in-situ methods have been proposed for estimating K_{sat} within the unsaturated (vadose) zone of the soil (Amoozegar and Warrick 1986), which include the following in-situ standard methods: (1) the constant-head (known also as the Amoozemeter), (2) the single or double ring infiltrometer, and (3) the rainfall simulator.

The constant-head method is based on maintaining a constant water head on an auger hole using a set of piezometer tubes, and measuring the volumetric rate of water needed to maintain this constant head (Amoozegar 1989). The method was used to measure subsurface saturated hydraulic conductivity and can also be used to measure K_{sat} of individual layers of a stratified soil (Amoozegar and Wilson 1999). The ring

infiltrometer method is based on ponding water within a cylindrical ring impeded in the soil surface and measuring the volumetric rate of water needed to maintain a constant head (Wu et al. 1999). The rainfall simulator is based on dripping water within a confined area under different intensities and measuring the volumetric rate of runoff from a single outlet (Elhakeem and Papanicolaou 2008). A complete guide and detailed discussion of these standard methods can be found in ASTM 1992n, and Amoozegar and Warrick (1986).

The method most closely related to this study's objective is the Double Ring Infiltrometer (DRI) and the Rainfall Simulator (RS) because they are used to measure K_{sat} in the vertical direction near the ground surface. Those two instruments were utilized throughout the United States with few, if any, adjustments to account for regional differences in climate or soil texture. Standardization makes these instruments widely acceptable and leads to the development of robust procedures for their application. The main difference between the two instruments is that DRI provides only point measurements of the baseline saturated hydraulic conductivity, K_b, while RS provides plot measurements of effective saturated hydraulic conductivity K_e. Therefore, the DRI, in most cases, accounts only for the intrinsic soil properties (e.g., soil texture), whereas the RS accounts for the intrinsic properties and extrinsic factors collectively. A detailed description of these two instruments and method of analysis is provided in Chapter 3.

2.2 Infiltration Models

2.2.1 The Pedotransfer Functions

Many infiltration models have been developed to predict the baseline saturated hydraulic conductivity, K_b (e.g., Bloemen 1980, van Genuchten 1980, Cosby et al. 1984, Brakensiek et al. 1984, Saxton et al. 1986, Vereecken et al. 1990, Campbell and Shiozawa 1994, Nearing et al. 1996). These models are known in the literature as the

pedotransfer functions (PTFs). Two approaches have been proposed for the development of a PTF. The first approach relates K_{sat} to soil properties such as clay, sand, and organic content, as well as bulk density via empirical equations and multivariate regression analysis (e.g., Brakensiek et al. 1984, Cosby et al. 1984, Saxton et al. 1986, Vereecken et al. 1990, Risse et al. 1995). Other advanced correlation techniques include fuzzy logic and neural network methods (e.g., Schaap 1998). The second approach relates K_{sat} to soil properties such as particle size distribution, porous structure, and water retention via physical and physio-empirical relationships (e.g., Bloemen 1980, van Genuchten 1980, Campbell and Shiozawa 1994). The latter approach requires input data that are not routinely collected by soil surveyors, which limits its application (Hipple et al. 2003, Tugel et al. 2005). Table 2.1 summarizes the mathematical expression for selected PTFs.

2.2.2 Watershed Models

Many physically-based, watershed models include empirical and rational infiltration equations that adjust K_b, to account for extrinsic factors such as rainfall, canopy cover, land use, management practices (e.g., Alberts et al. 1988, Potter 1990, Rawls et al. 1990). Common models which account for extrinsic factors to predict the effective hydraulic conductivity, K_e, are: KINEROS (Smith et al. 1995); MIKE-SHE (Refsgaard and Storm 1995); WEPP (Nearing et al. 1996); SWAT (Arnold et al. 1998); and GSSHA (Downer and Ogden 2002); CAESAR (Coulthard et al. 2002).

Risse et al. (1995) proposed a rational equation to account for the role of landform surface roughness, surface crust, and raindrop impact on K_b. The equation was expressed as

$$K_{br} = K_b[CF + (1 - CF)e^{-C \cdot E_a (1 - RR_t / RR_{r-\max})}] \quad (2.1)$$

where K_{br} (mm/h) is bare saturated hydraulic conductivity that takes into account the effects of crusting and tillage, K_b (mm/h) is baseline hydraulic conductivity, *CF* is the crust factor, *C* is soil stability factor (m^2/J), E_a (J/m^2) is the cumulative rainfall kinetic energy since the last tillage, RR_t is random roughness (m), and $RR_{t\text{-}max}$ is the maximum random roughness.

The *CF* was found to be a function of the capillary potential at the crust/sub-crust interface, partial saturation of the sub-crust soil, and the wetting front depth (e.g., Green and Ampt 1911, Morin et al. 1989). Typical *CF* values are between 0.2 and 1.0. The soil stability factor *C* is a function of the soil texture and cation exchange capacity (*CEC*). Reported *C* values in the literature are between 0.0001 and 0.01 (Bosch and Onstad, 1988). Potter (1990) has shown that the RR_t obtained a value of about 0.04 m immediately after the last tillage, which corresponds to $RR_{t\text{-}max}$. The study showed also that RR_t decreases exponentially with time. The cumulative rainfall kinetic energy E_a can be calculated from the following equation (Salles et al., 2002):

$$E_R = E_a / T_R = 1288.17\alpha^{-1.34} I^{1+1.34\beta} \tag{2.2}$$

where T_R (hr) is the total rain time, E_R [$J/(m^2 \cdot h)$] is the rainfall kinetic energy, *I* is the rainfall intensity (mm/h), and α and β are the regression parameters depending on the rainfall intensity, which have average values of 35 and 0.13, respectively.

Vegetation cover (canopy and residue) (Khan et al. 1988) and single storm rainfall (Onstad et al. 1984) were found to alter K_{br}. While vegetation cover reduces field infiltration rate, Wischmeier (1966) found that large storms increase infiltration rate. The saturated hydraulic conductivity accounting for the collective effects of vegetation cover and single storm events can be expressed as (Kidwell et al. 1997):

$$K_e = K_{br}\left(1 - C_{TE}\right) + \left(0.0534 + 0.01179 K_b\right) C_{TE} P \tag{2.3}$$

where P is the storm rainfall amount (mm) and C_{TE} is the total effective surface cover that is related to the fractions of the canopy and residue within the field as (Khan et al. 1988):

$$C_{TE} = C_{CE} + C_{RE} - C_{CE}C_{RE} \quad (2.4)$$

where C_{RE} is the effective residue cover that ranges from 0 to 1, and C_{CE} is the effective canopy cover as a function of the crop height and the area occupied by the crop leaves. For the fallow case, equation (2.3) reduces to $K_e = K_{br}$.

2.3 Data Interpolation

The field methods and infiltration models described to this point were developed for K_{sat} estimates from point or at best plot data. Integration of the data over scales larger than what these methods and model provide requires interpolation via geospatial techniques. Several interpolation methods are available depending on the nature of the interpolated data. One of these methods is the Thiessen (known also as Dirichlet or Voronoi) polygons, which takes the classification model of spatial prediction to the extreme whereby the predictions of attributes at unsampled locations are provided by the nearest single data point (Bolstad 2008). Thiessen polygons divide a region up in a way that is totally determined by the configuration of the data points, with one observation per cell. As a consequence, the data are assumed to be homogeneous within the polygons and change values only at the boundaries. Therefore, this method is often used in Geographic Information System (GIS) for qualitative data like vegetation classes or land uses.

For data that do not spread uniformly over a region (a polygon) but tend to congregate in certain parts, Tobler (1979 and 1995) proposed a method, known as pycnophylactic interpolation, which is based on a mass-preserving reallocation from primary data. The method ensures that the volume of the attribute (e.g., number of soil textures or other attributes) in a spatial entity (polygon or administrative area) remains

the same, irrespective of whether the global variation of the attribute is represented by homogeneous, crisp polygons or a continuous surface. The method removes the abrupt changes at the boundaries of the polygons providing a more realistic representation to the data distribution by a smooth surface. The primary condition for mass preservation is:

$$\int_{R_i} \int f(x, y) dxdy = V_i \tag{2.5}$$

for all i, where V_i denotes the value (e.g., soil texture) in region R_i.

Equation (2.5) indicates that the total volume of the attribute (e.g., soil texture) per polygon is invariant whether the soil texture is formed by a uniform polygon with crisp boundaries or by a smooth, continuous surface that takes account the soil texture differences in the neighboring areas. The constraining surface is assumed to vary smoothly so that neighboring locations have similar values (Tobler 1995). Unless there are physical barriers, the densities in neighboring areas tend to resemble each other and so a joint, smooth surface is fitted to contiguous regions. The simplest method to satisfy the model constraints is to use the Laplacian condition, i.e. by minimizing:

$$\int_R \int \left(\frac{\partial f^2}{\partial x} + \frac{\partial f^2}{\partial y} \right) dxdy \tag{2.6}$$

where R is the set of all regions. The most general boundary condition is:

$$\frac{\partial f}{\partial \eta} = 0 \tag{2.7}$$

which constrains the gradient of the fitted surface perpendicular to the edge of the region to be flat (η indicates the boundary between regions).

Inverse distance methods of interpolation combine the ideas of proximity espoused by the Thiessen polygons with the gradual change of the under investigation variable (Liszka 1984). The assumption is that the value of an intrinsic factor, for

example, at some unvisited point is a distance-weighted average of data points occurring within a neighborhood or window surrounding the unvisited point. Typically, the original data points are located on a regular grid or are distributed irregularly over an area and interpolations are made to locations on a denser regular grid in order to make a map. The weighted moving average methods compute:

$$\hat{z}(x_j) = \sum_{i=1}^{n} \lambda_i \cdot z(x_i) \; ; \; \sum_{i-1}^{n} \lambda_i = 1 \tag{2.8}$$

where the weights λ_i are given by $\Phi(\mathrm{d}(x, x_i))$. A requirement is that $\Phi(d) \rightarrow$ the measured value as $d \rightarrow 0$, which is given by the commonly used negative exponential functions e^{-d} and e^{-d^2}. The most common form of $\Phi(d)$ is the inverse distance weighting predictor that its form is:

$$\hat{z}(x_j) = \sum_{i=1}^{n} z(x_i) \cdot d_{ij}^{-r} \Big/ \sum_{i=1}^{n} d_{ij}^{-r} \tag{2.9}$$

where the x_i and x_j are the data points and the points where the surface is to be interpolated, respectively.

Because in Equation 2.9, $\Phi(d) \rightarrow 0$ as $d \rightarrow 0$, the value for an interpolation point that coincides with a data point must be simply copied over. The simplest form of this is called the linear interpolator, in which the weights are computed from a linear function of distance between sets of data points and the point to be predicted.

Inverse distance interpolation is commonly used in GIS to create raster which overlays from point data (Kravchenko et al. 2000). Once the data are on a regular grid, contour lines can be threaded through the interpolated values and the map can be drawn as either a vector contour map or as a raster shaded map. Due to its advantages and relevance to our application, inverse distance interpolation will be the method adopted in our study.

Table 2.1 Mathematical expression for selected PTFs

Author	PTF mathematical expression ($K_b : mm/hr$)
Cosby et al. (1984)	$K_b = 25.4 \times 10^{(-0.6+0.0126Sa-0.0064Cl)}$
Rawls and Brakensiek (1985)	$K_b = 10\exp[19.52348p - 8.96847 - 0.028212Cl + 1.8107\times10^{-4}Sa^2 - 9.4125\times10^{-3}Cl^2 - 8.395215p^2 + 0.077718Sa\times p - 0.00298Sa^2\times p^2 - 0.019492Cl^2\times p^2 + 1.73\times10^{-5}Sa^2\times Cl + 0.02733Cl^2\times p + 0.001434Sa^2\times p - 3.5\times10^{-6}Cl^2\times Sa]$
Saxton et al. (1986)	$K_b = 10\exp[12.012 - 7.55\times10^{-2}Sa(-3.865 + 3.671\times10^{-2}Sa - 0.1103Cl + 8.7546\times10^{-4}Cl^2)/p]$
Vereecken et al. (1990)	$K_b = 0.416664\exp[20.62 - 0.96\ln(Cl) - 0.66\ln(Sa) - 0.46\ln(OM) - 8.43\ln(BD)]$
Jabro (1992)	$K_b = 10\times10^{[9.56-0.81\log(Si)-1.09\log(Cl)-4.64BD]}$
Dane and Puckett (1994)	$K_b = 303.84\exp(-0.144Cl)$
Campbell and Shiozawa (1994)	$K_b = 54\exp(-0.07Sa - 0.167Cl)$
Risse et al. (1995)	$K_b = 10\times(-0.265 + 0.0086Sa^{1.8} + 11.46CEC^{-0.75})$
Wosten et al. (1999)	$K_b = 0.416664\exp[8.685 + 0.0352Si - 0.967BD^2 - 0.000484CL^2 - 0.000322Si^2 + 0.001Si^{-1} - 0.0748OM^{-1} - 0.0643\ln(Si) - 0.01398BD\times Cl - 0.1673BD\times OM + 0.02986Cl - 0.03305Si]$
Rosetta BD – Schaap (1999)	Neural network requiring Cl , Si , Sa and BD
Rosetta – Schaap (1999)	Neural network requiring Cl , Si , and Sa

(Note: Cl = % of clay content, Si = % of silt content, Sa = % of sand content, BD = bulk density (gm/cm^3), p = prosity, OM = % organic matter content, and CEC = cation exchange capacity (meq/100gm).)

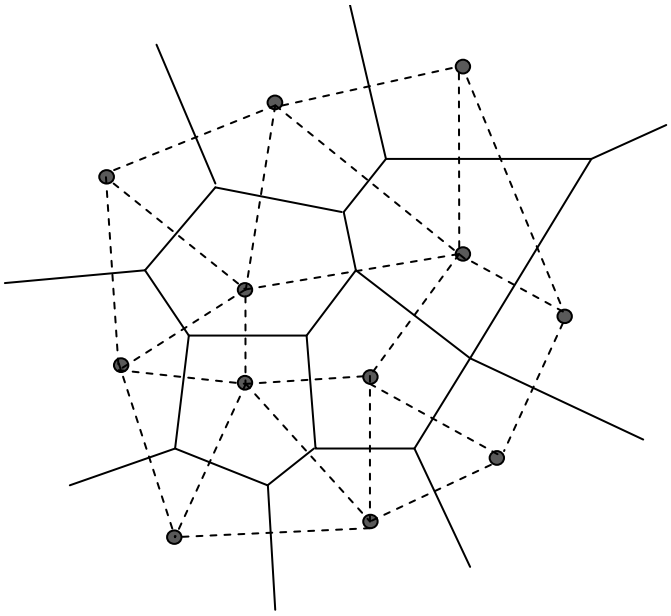

Figure 2.1 An example of a Thiessen polygon net and the equivalent Delaunay triangulation.

CHAPTER 3 METHODOLOGY

The methodological steps needed to accomplish the study objectives include:

1) The performance of field measurements using automated DRIs and RSs to calibrate and validate the models.

2) Integration of the PTFs and watershed models with the geospatial tools to develop a physically-based modeling framework within which different geographic, climatic, and land use data can be incorporated.

3.1 Field Measurements

This section describes the field methods used for conducting in-situ K_{sat} measurements using automated double ring infiltrometers (DRIs), and rainfall simulators (RSs). The DRI provides only point measurements of the baseline saturated hydraulic conductivity, K_b, while RS provides plot measurements of effective saturated hydraulic conductivity, K_e. Thus, the DRI, in most cases, accounts only for the intrinsic soil properties (e.g., soil textures and bulk density), whereas the RS accounts for the intrinsic properties and extrinsic factors collectively. Both K_b and K_e measurements were needed for model calibration and verification.

3.1.1 Study Site

Infiltration measurements were conducted in a representative watershed in southeastern Iowa, namely the South Amana Subwatershed (SAS) in the Clear Creek Watershed (CCW), Iowa (Figure 3.1a). SAS is located in the northwest corner of CCW and encompasses approximately 10% of the total CCW drainage area, which is about 270 km^2. The SAS has two sub-basins, both containing first order tributaries. Each

tributary is approximately 6 river km long during the wet season. The outlet of the SAS is approximately 30 river km upstream of the Clear Creek - Iowa River confluence.

The SAS is entirely in the Southern Iowa Drift Plain (Prior, 1991) and lies within Major Land Resource Area (MLRA) 108C, Illinois and Iowa Deep Loess and Drift, West Central Part (USDA-NRCS, 2008a). Peorian loess is always found on summits, where it can be 10 *m* thick (Ruhe, 1969). On some hills, the loess extends to the footslope – where its thickness is consistently greater than 2 m grading into thick silty colluvium, then into thick silty alluvium on the lower toeslope. On other hills, the loess pinches out on the shoulder or backslope, exposing both/either a Yarmouth-Sangamon Paleosol and/or Pre-Illinoian till. More commonly, the paleosol, or till, is under a few centimeters up to two meters of loess and silty colluvium. On hills where the paleosol is exposed, footslopes may be dominated by loamy or silty textured colluvium. Most valleys are filled with Holocene aged silty alluvium. In other words, the Pleistocene stratigraphy across these landscapes is simple, albeit variable, in thickness. These resulted in a complex spatial variety of texture, bulk density, and water holding capacity for the soil series being mapped.

There are four main soil series mapped across the SAS (USDA-NRCS, 2008b, 2008c) comprising approximately 80% of the total acreage (Figure 3.1b). The uplands are comprised of the Tama series, which is the most prominent in the southern sub-basin, and the Downs series, which is prominent in the northern sub-basin. Both soils are well-drained and are formed from Peorian loess. They are respectively considered the end members of a prairie-forest biosequence. Floodplains are comprised of mostly Ely and Colo soil series. These soils are derived from alluvium. The Ely and Colo soils are poorly drained. Table 3.1 summarizes the classifications of different soil series. Some of the highest erosion rates in the CCW have been observed within the SAS, mainly due to a combination of swelling and highly erodible soils with steep slopes and

intensive tillage. The average slope is 4% with a range that varies from 1% to 10%. Figure 3.2 shows a representative look at the aerial map of the SAS.

Currently in the SAS, there are nine main land uses. Six of the land uses represent various corn-soybean rotations. Each rotation involves a unique set of the following management practices: no-till, reduced spring tillage, and conventional fall tillage with secondary tillage in the spring. Three of these rotations encompass over 80% of the watershed acreage. Hay farming, pastures, and fields enrolled in the Conservation Reserve Program (CRP) are the remaining land uses. The growing season lasts about 180 days in Southeast Iowa.

Due to the mid-continental location of Iowa, the SAS climate is characterized by hot summers, cold winters, and wet springs (Highland and Dideriksen, 1967). Summer months are influenced by warm, humid air masses from the Gulf of Mexico, while dry Canadian air masses dominate the winter months. Average daily temperature is about 10^{o}C, ranging from an average July maximum of 29°C to an average January minimum of -13°C. Average annual precipitation is approximately 889 mm/yr with convective thunderstorms prominent in the summer, and snowfall in the winter, which averages 762 mm annually.

3.1.2 Test-bed Matrix

An important element in the field component of this study was the development of an experimental test-bed matrix within the SAS that incorporated: (1) the selection of the test fields based on soil series, land use, and management practices; (2) the determination of the number of measurements and locations in each field that can provide statistically defendable estimates of K_{sat}.

Three fields were selected to represent different soil series, and management practices in the SAS. These fields were: the conventional tillage soybean (CT-SB), the

no-till soybean (NT-SB), and the conservation reserve program (CRP). The measurements were conducted in the summer and fall of 2009 to identify the role of rotation on K_{sat} and to test the repeatability of the results.

The spatial arrangement of the double ring infiltrometer (DRI) in each field was designed to eliminate any possible sources of bias that may occur from causal connection (i.e., high correlation) between neighboring measuring locations. A second order invariant correlation function (e.g., Witten and Sander, 1981) was used to examine the independency of the measurements and was expressed as follows:

$$T(\Delta x, \Delta y) = \frac{1}{(m-\Delta x)(n-\Delta y)} \sum_{i=1}^{m-\Delta x} \sum_{j=1}^{n-\Delta y} \rho(i, j)\rho(i+\Delta x, j+\Delta y) \quad (3.1)$$

where, m and n are the number of measurements in the x and y directions, respectively, Δx and Δy are the lags between the measurements in the x and y directions, respectively, $\rho(i, j)$ is a density function that defines K_{sat} and the corresponding properties. Theoretically, $\rho(i, j)$ is equal to 1.0 when K_{sat} is constant within the field, and 0.0 when K_{sat} is variable within the field. To determine the optimal spacing between the measurements, the critical value for low correlation between the measurements (i.e., no causal connection exist) was set to $T < 0.25$. This critical T value corresponded to an average spacing varies between 10 to 15 meters, or equivalently 30 to 50 measurements per field. This number of measurements is the minimum suggested range for statistical representation and analysis of the data (Shahin et al., 1993). Figure 3.1c shows the measurement locations in each field obtained via a Trimble GeoExplorer-3 GPS and integrated into ArcGIS database (ESRI Redlands, CA). In Figure 3.1c, the circles show the DRI measurement and core sampling locations of this study, while the small dots show the DRI measurement locations from previous studies (Papanicolaou et al., 2008). The black rectangles in Figure 3.1c correspond to the locations of the rainfall simulator

(RS) measurements. Table 3.2 summarizes the variables and number of measurements per field conducted in this study.

3.1.3 K_{sat} Measurements and Method of Analysis

The field experiments were conducted in summer and fall of 2009 during periods of stable weather conditions, i.e., minimal variation in temperature and soil moisture condition. Periods of freeze-thaw cycles were avoided to minimize the errors resulting from soil aggregates breaking. A water quality analysis was conducted for metals and pH of the supply water, which may affect the cohesion and porous structure of the soil, thereby altering the infiltration rate. The analysis showed that the properties of the supply water were close to Iowa natural rainfall properties.

K_{sat} was measured in-situ using two infiltration instruments, namely the semi-automated Double Ring Infiltrometer (DRI), and the Rainfall Simulator (RS). These instruments were automated by the IIHR-Hydroscience and Engineering at the University of Iowa. The automation process allowed for continuous operation of multiple sensors simultaneously for sufficient durations (up to 200 hrs of continuous recording, if needed) to reach the steady state condition. Description of each device principle, components, operation procedure, and methods of data analysis is presented below:

(1)The Double Ring Infiltrometer

The DRI measures the vertical saturated hydraulic conductivity (K_{sat}) within the top 15 to 30 cm (6 to 12 in) of the soil surface. It consists of two concentric rings as shown in Figure 3.3. The outer ring forms a buffer compartment around the inner ring to control lateral flow. Thus, allows for measurement of vertical infiltration in the inner ring.

IIHR-Hydroscience and Engineering has a total of thirty automated DRIs that can be operated simultaneously with minimum labor. The semi-automated DRI kit [figure 3.4(a) and 3.4(b)] includes: a five gallon water tank hung from a tripod connected to a control valve with an adjustable tube to feed the inner ring; a data-logger (time recorder) operated via a 12 volt battery; and a five gallon Mariotte bottle to maintain constant water head in the outer ring. Figure 3.5(a) and 3.5(b) shows the set-up of the DRIs in the CRP field.

The experimental procedure for operating the DRI was as follows: the rings were hammered into the ground 5 to 10 cm (2 to 4 in) with minimum disturbance and filled with water to an initial ponding depth 5 to 8 cm (2.0 to 3.0 in). A constant water level was maintained in the outer ring with the Mariotte bottle. The water level in the inner ring was allowed to drop by 1.0 cm (0.5 in) from the initial ponding depth before refilling of the inner ring. The time required for the water level to drop 1.0 cm was recorded continuously by a data-logger.

The infiltration curve (figure 3.6) was plotted from the infiltration rates (f). The infiltration rate was calculated using the following equation:

$$f = \frac{\Delta V}{A \Delta t} \tag{3.2}$$

where, ΔV is the volume of water added to the inner ring during time interval Δt, and A denotes the cross-sectional area of the inner ring. K_{sat} was obtained at the steady infiltration rate (figure 3.7). Table A1 in Appendix A provides the measured K_{sat} from the DRIs and the time needed to reach the steady state condition.

(2)The Rainfall Simulator

The RS provides an average K_{sat} value over a small plot area. The IIHR-Hydroscience and Engineering at the University of Iowa has three Norton Ladder

Multiple Intensity Rainfall Simulators) manufactured by the USDA-ARS National Soil Erosion Research Laboratory in W. Lafayette, IN. The basic unit of each simulator consists of an aluminum frame 2.5 m long, 1.5 m wide, and 2.7 m high. The frame has 4-telescopic legs to maintain stability and vertical orientation of the nozzles. The frame was a self-contained unit that includes 2-nozzles spaced 1.1 m apart, piping, an oscillating mechanism, and a drive motor. The nozzles (Figure 3.7a) provided a median drop size of 2.25 mm, an exit velocity of 6.8 m/s, spherical drop shape, and a maximum rainfall intensity of 135 mm/hr. The simulators rainfall intensity can be changed instantaneously from a controller during a simulation event. The simulators were equipped with storage tanks and a water pump with a system of valves that allowed rainfall intensity to be adjusted for each simulator independently. Galvanized metal sheets (Figure 3.7a) were used for plot borders. Wind shields (Figure 3.7a) comprised of slightly porous- fabric sheets were used to inhibit wind influence.

The experimental procedure to conduct the RS experimental runs was as follows: the RS was installed at the selected fields with minimum disturbance. The RS was set to certain rainfall intensity and the runoff was collected from the outlet of the plot via small calibrated bottles from a small pipe connected to the metal sheets (Figure 3.7b). The rainfall intensity was increased until the runoff reaches a steady state condition. The infiltration rate f (L/T) was determined through the following equation:

$$f = I - q \tag{3.2}$$

where I is the rainfall intensity (L/T) and q is the runoff rate (L/T).

Figure 3.8 indicates that the infiltration rate has reached a steady state condition through the RS measurements. This steady state infiltration rate determines the K_{sat}. Table A2 in Appendix A provides the measured K_{sat} from the RSs and the time needed to reach the steady state condition. The trend of the data shown in Figure 3.8 should not be

confused with the typical plot shown in Figure 3.6 because the x-axis is different in the two figures. In figure 3.6 is time, whereas in figure 3.8 is rainfall intensity.

3.1.4 Soil Characterization

A total of 10 soil cores, with a 7.5 cm (3 inches) diameter and 2.0 m (7 ft) depth, were collected in the vicinity of the measured K_{sat} locations from each test field via a truck-mounted Giddings Probe for soil characterization (figures 3.9a and 3.9b). The landscape positions were identified at the sampled locations using the hillslope model of Ruhe (1969). Characterization of soil texture was described in the Iowa State University Pedometrics Laboratory and at the field using a combination of standard soil morphological description methods (Soil Survey Staff 1998; Driese et al. 2001; Schoeneberger et al. 2002). These methods included physical characterization of soil horizons, soil texture, root extent, color, sedimentary structures, fracture density, and any other macroscopic features.

Fractions of clay, silt and sand are obtained from standard sieve and hydrometer analysis (Soil Survey Staff 1996). Bulk density values are measured on small (20~60 cm^3) undisturbed sub-samples using the wax clod method (Blake and Hartge 1986; Soil Survey Staff 1996; Konen 1999) and bulk porosity values are calculated using the bulk density values and assuming a specific gravity of 2.65 for the soil solids. Soil biogeochemical properties are determined for some horizons. This includes the soil pH, cation exchange capacity (*CEC*), water stable aggregate content (*WSAC*), and organic matter content (*OM*). Soil pH is determined using both a 1:1 soil to water mix and a 1:2 soil to 0.01M KCl solution (Soil Survey Staff 1996). *CEC* is determined by ammonium displacement of calcium as described by Jaynes and Bigham (1986) although the method of displacement is via shaking and centrifugation (Soil Survey Staff 1996). Organic matter is determined in the Iowa State Soil Testing Laboratory using the dry combustion

method described by Soil Survey Staff (1996) with a Leco LC2000 (Model CHN 600, LECO, St. Joseph, MI). *WSAC* is determined by the method of Patton el al. (2001).

Seven soil series were identified within the sampling regions of the three fields with the associations of Tama-Muscatine-Downs and the Otley-Ladoga series to be the most ubiquitous. Table 3.2 summarizes the soil composition of different soil series reported in the fields (USDA-NRCS 2008c).

3.2 Modeling Framework Development

A physically-based, modeling framework within which different geographic, climatic, and land uses data can be incorporated was developed by integrating selected PTFs and watershed models with geospatial tools to predict K_{sat} dynamics. Selection of the appropriate PTFs and watershed models that provide consistent predictions with the field measurements was based on statistical criteria. The PTFs predictions were compared to the DRI measurements, while the watershed models predictions were compared to the RS measurements. The selected PTF and watershed model were integrated with the Geographic Information System (GIS) tools by developing a program that facilitates the compilation of different geographically distributed data from registries of the data sources and computational resources of the selected models into GIS platform.

3.2.1 Models Selection

The first step towards developing the modeling framework is the selection of the appropriate models that represent the study site conditions (Vieux 2004). The models were examined against the field measurements of this study and the data collected from previous studies by Papanicolaou et al. (2008, 2009). The accuracy (the deviation between observed and predicted values) of a number of PTFs and watershed models was

examined through statistical measures of the models' errors (Shahin et al. 1993). Standard criteria such as the root mean square error (*RMSE*) and Akaike Information Criterion (AIC) were considered in this study to evaluate each model's performance [Scokaert et al. 1974; American Society of Civil Engineers (ASCE) 1993; Kirnak 2002]. Table 3.3 summarizes the selected statistical mean error criteria used for model evaluation.

The RMSE is a quadratic scoring rule which measures the average magnitude of the error. RMSE is the square root of the sample average by calculating the difference between predicted and corresponding observed values, squaring and then averaging over the samples. RMSE is most useful when large errors are particularly undesirable. The AIC is a measure of the goodness of fit of an estimated statistical model. It describes the tradeoff between bias and variance in model construction, and the precision and complexity of the model. The AIC is a tool for model selection. Given a data set, several competing models may be ranked according to their AIC. Both the RMSE and AIC are negatively-oriented scores that range from 0 to ∞. The lower their values, the closer the agreement between the predicted and measured values. The GMER and the GSDER were also considered in the evaluation to account for the log-tailed distribution of K_{sat} (Papanicolaou et al. 2008). The predicted values are overestimated if GMER>1.0 and underestimated if GMER< 1.0. Perfect agreement between the predicted the measured values is obtained when the GSDER=1.0.

The predicted K_{sat} from the PTFs is defined as the baseline saturated hydraulic conductivity, K_b. The main assumption underlying most PTFs is that textural properties dominate the hydraulic behavior of soils (e.g., Risse et al. 1995; Schaap et al. 2001). As a result, PTFs are often used in geographic and climatic regions different from the one, for which they were originally developed, without calibration and validation. This can produce large errors in K_b values calculated from these PTFs. Therefore, the predictions of the 12 PTFs, described in Chapter 2, were evaluated against the available field data of

the South Amana Subwatershed (SAS) to identify the most suitable PTF for the modeling framework. Watershed models that account for extrinsic factors typically adjust the values of K_b, obtained from the PTFs, for variables such as vegetation, land use, management practices, and precipitation. The predicted K_{sat} from these models is defined as the effective hydraulic conductivity, K_e. The main assumption underlying most of these models is that extrinsic factors can alter K_{sat} values for soils exhibiting the same surface texture (e.g., Smith et al. 1995; Nearing et al. 1996). The predictions of four watershed models were evaluated against the available field data collected from the SAS to identify the most suitable model for the modeling framework.

Table 3.4 summarizes the performance of the PTFs and watershed models. The overall performance of the PTFs and watershed models were evaluated using the following scoring rule: one point was assigned for each criterion shown in Table 3.4 to give a total of seven points. The scores were relative on a linear scale and based on the close agreement between the measured and predicted values. The score for the different PTFs is given in Table 3.4 along with the total score. The last column in the table shows the overall performance in percentage. The table shows that Rosetta and WEPP predictions provided the best agreement to the measured K_{sat} values in the SAS. Therefore, Rosetta and WEPP were used in the modeling framework to obtain K_b and K_e, respectively, in this study. Figure 3.10 shows the process used to calibrate Rosetta and WEPP. A brief description of both models and the supplementary equations and tables needed to calculate K_e is given in Appendix B.

3.2.2 Models Integration

Rosetta and WEPP were integrated with the GIS tools to develop a physically-based, modeling framework within which different geographic, climatic, and land use data can be incorporated. ArcGIS, developed by the Environmental Systems Research

Institute (ESRI), Redlands, CA, was used for graphical representation of the models outputs. The modeling framework allowed for visualization of the data in forms of geospatial maps for the prediction of K_{sat} dynamics.

Geospatial data for both Rosetta and WEPP models were obtained from open-access Internet sources. An algorithm was developed to facilitate the compilation of different geospatially distributed data from registries of the data and computational resources of the models into the ArcGIS interface (Figure 3.11). The data were downloaded, transmitted to the computational resources of the models, and converted with the developed code into a format that can be implemented into ArcGIS. The developed program for data registries is given in Appendix C. ArcMap, a subcomponent of ArcGIS, was used to convert the soil vector maps into raster maps, develop maps for different variables describing the models, and convert the raster maps into data points for statistical analysis.

Soil, land use, and precipitation data were collected from different databases as inputs for Rosetta and WEPP. The soil data were obtained from the Soil Survey Geographic (SSURGO) databases of the Natural Resources Conservation Service (NRCS) and the Iowa Department of Natural Resources (IDNR). The databases provide information regarding the soil series, major soil area, taxonomic classification (order and suborder), hydrological group, soil textures, surface and subsurface bulk density, organic matter, cation exchange capacity (*CEC*), and soil pH. Detailed maps of land uses and management practices of the Clear Creek Watershed (CCW) were obtained from IDNR. The precipitation depth and intensity were obtained from the Iowa Environmental Mesonet (IEM) of the Department of Agronomy at the Iowa State University. The collected data from these databases were incorporated into Rosetta and WEPP, and imported as layered information into ArcGIS to generate K_{sat} dynamic maps for the entire Clear Creek Watershed. Figure 3.12 shows the variables needed from different databases

for Rosetta and WEPP to predict baseline, bare, and effective saturated hydraulic conductivities (K_b, K_{br}, and K_e), which were described in section 2.2.

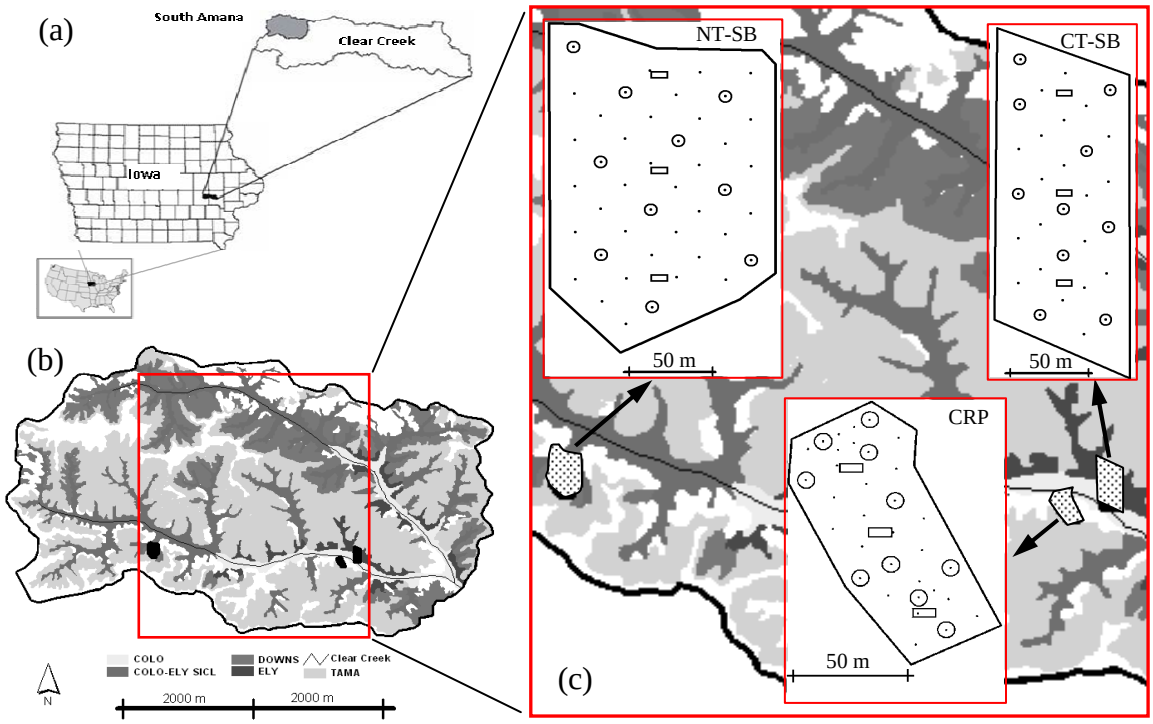

Figure 3.1 The South Amana Subwatershed (SAS): (a) geographical location; (b) major soil types and test fields location; (c) measuring locations in the test fields: CRP (NE ¼ SE ¼ section 18, T80N, R9W); CT-SB (NW ¼ SW ¼ section 17, T80N, R9W); NT-SB (NW ¼ SW ¼ section 13, T80N, R10W).

Table 3.1 Series of soil map units within the sampling region of the three fields.

Series	Classification	CRP	CT-soybean	NT-soybean
Colo	Fine-silty, mixed, superactive, mesic Cumulic Endoaquoll		×	×
Downs	Fine-silty, mixed superactive mesic Mollic Hapludalf			×
Ely	Fine-silty, mixed, superactive, mesic Aquic Cumulic Hapludoll		×	×
Judson	Fine-silty, mixed, superactive, mesic Cumulic Hapludoll	×		
Otley	Fine, smectitic, mesic Oxyaquic Argiudoll			×
Shelby	Fine-loamy, mixed, superactive, mesic Typic Argiudoll	×		
Tama	Fine-silty, mixed superactive mesic Typic Argiudoll	×	×	×

Source: USDA-NRCS, 2008

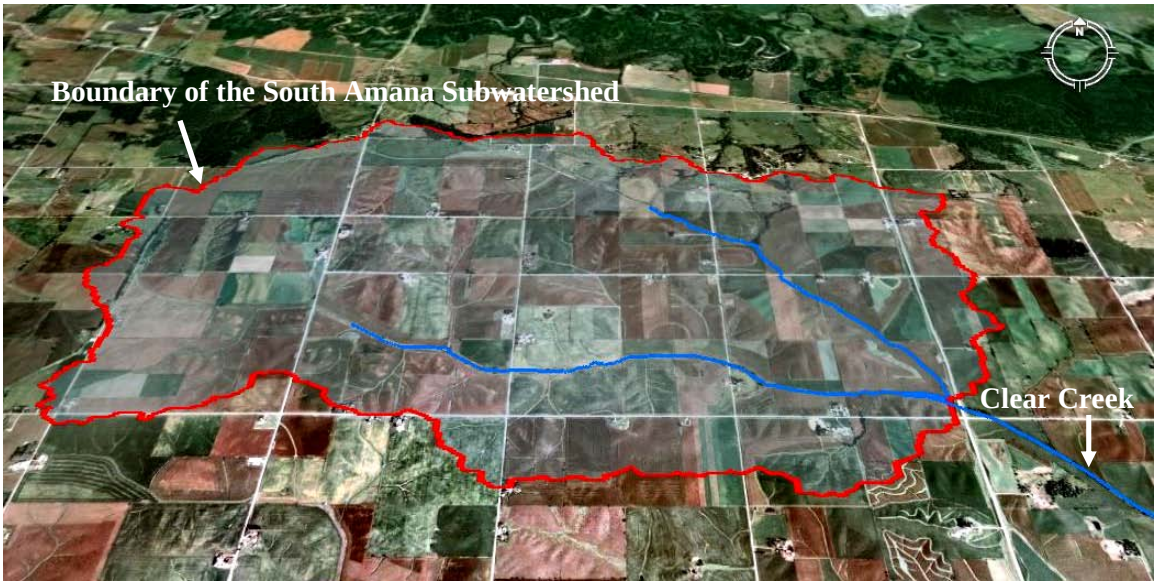

Figure 3.2 Aerial map of the South Amana Subwatershed, IA.

Table 3.2 Test-bed matrix: experimental variables and number of measurements.

Instrument	Variable	Field						Total number of measurements
		CRP		CT-soybean		NT-soybean		
		Number of measurements per season						
		S**	F**	S	F	S	F	
DRI	K_b*	10	10	10	10	10	10	58
	Time to steady state condition	10	10	10	10	10	10	58
RS	K_e*	36	18	36	18	36	18	216
	Time to steady state condition	3	3	3	3	3	3	18

* Average K_{sat} values at 3 locations in each field from 12 and 6 runoff measurements in summer and fall, respectively.
**S = summer, F=fall

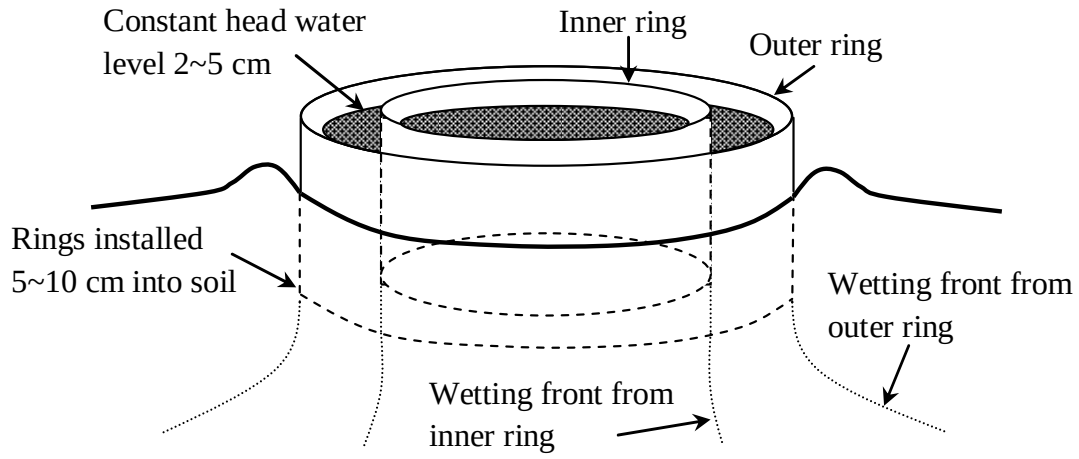

Figure 3.3 The University of Iowa Double Ring Infiltrometer – operational condition.

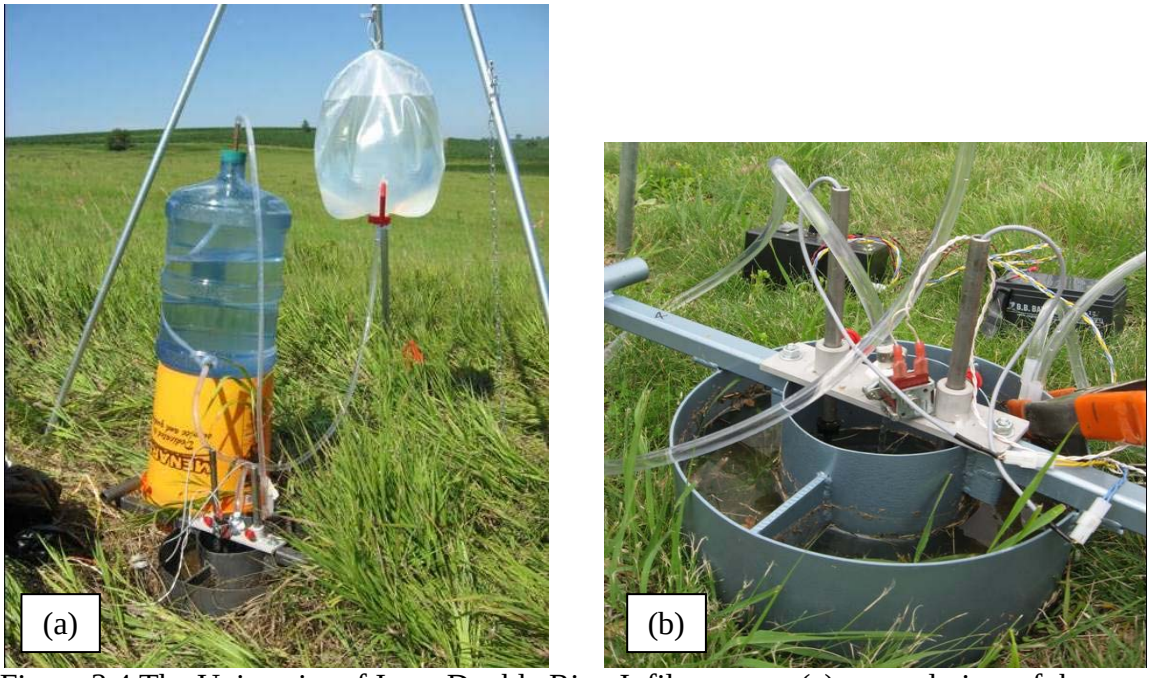

Figure 3.4 The University of Iowa Double Ring Infiltrometer: (a) general view of the setup; (b) close view of the sensors.

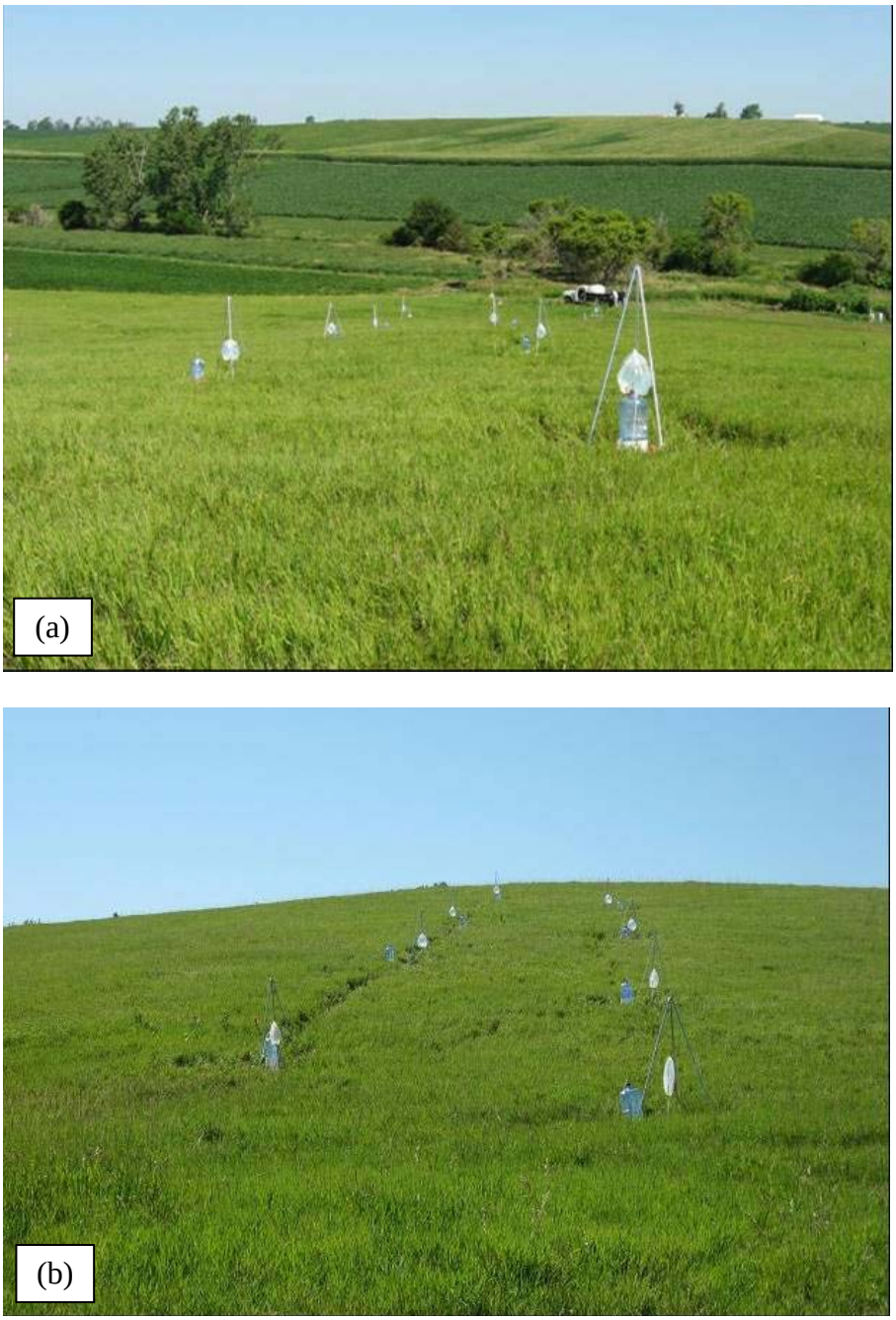

Figure 3.5 Set-up of the DRIs in the CRP field.

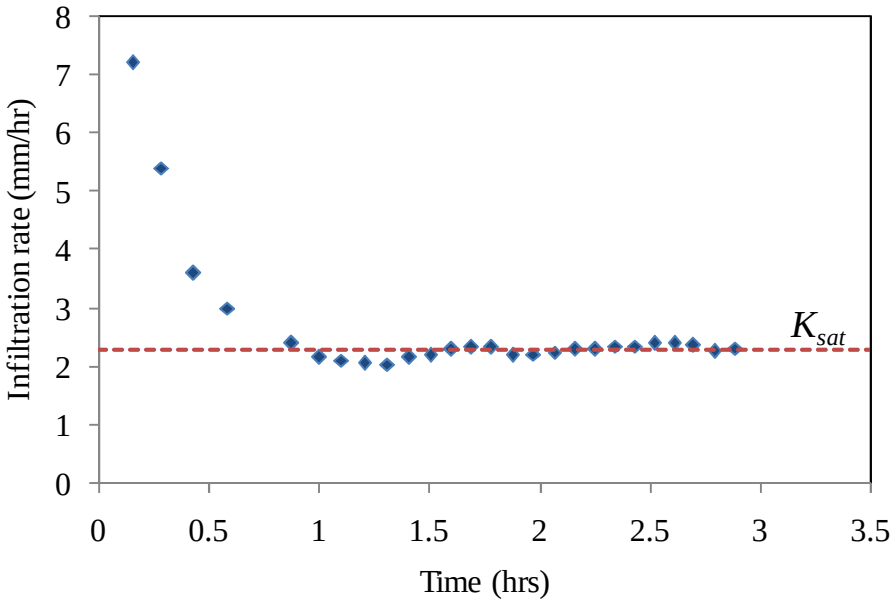

Figure 3.6 Results of the DRI measurements in the SAS.

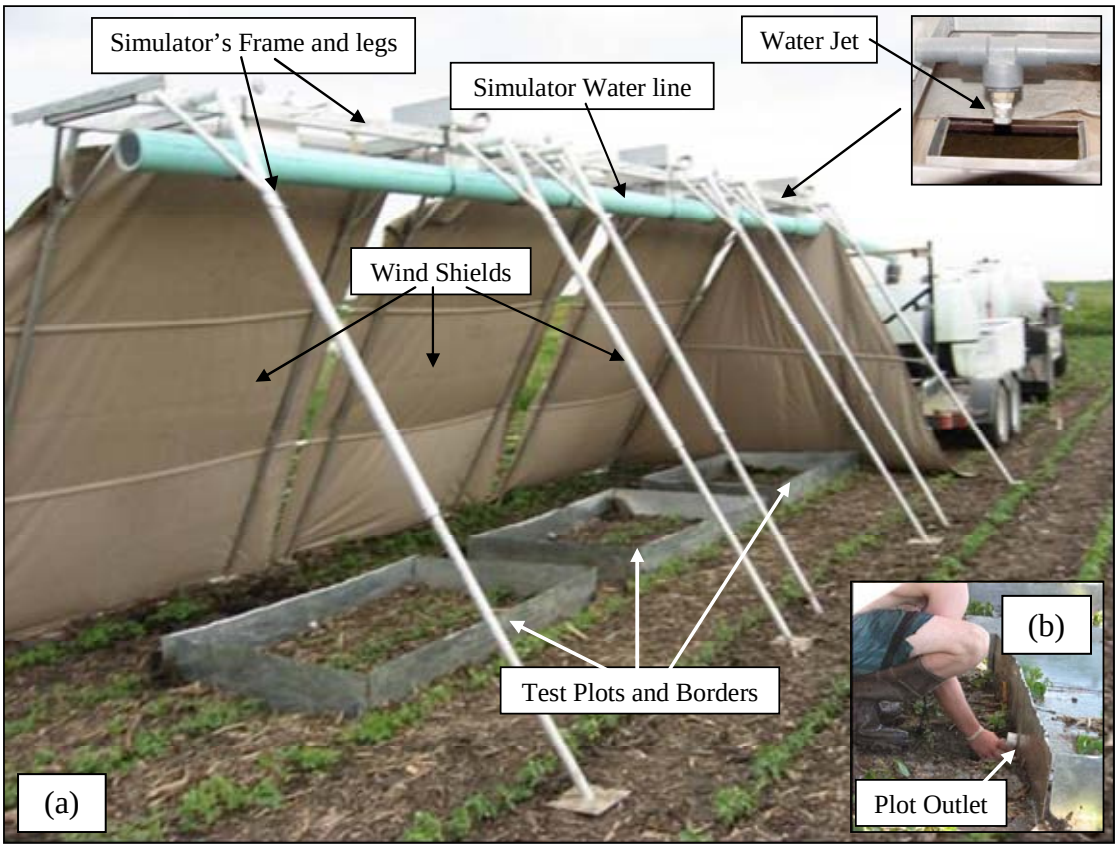

Figure 3.7 The University of Iowa Rainfall Simulator: (a) general view; (b) surface runoff collection.

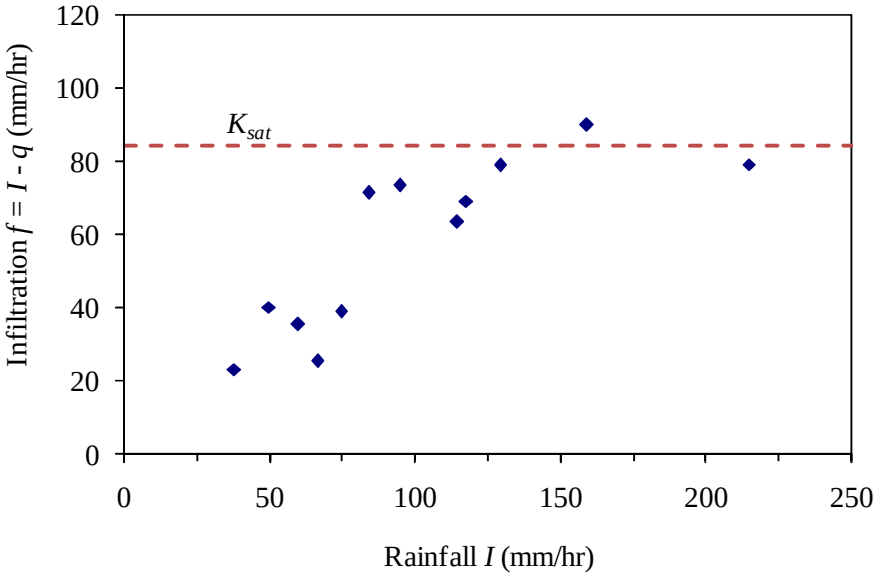

Figure 3.8 Example of the measurement result of the University of Iowa Rainfall Simulator.

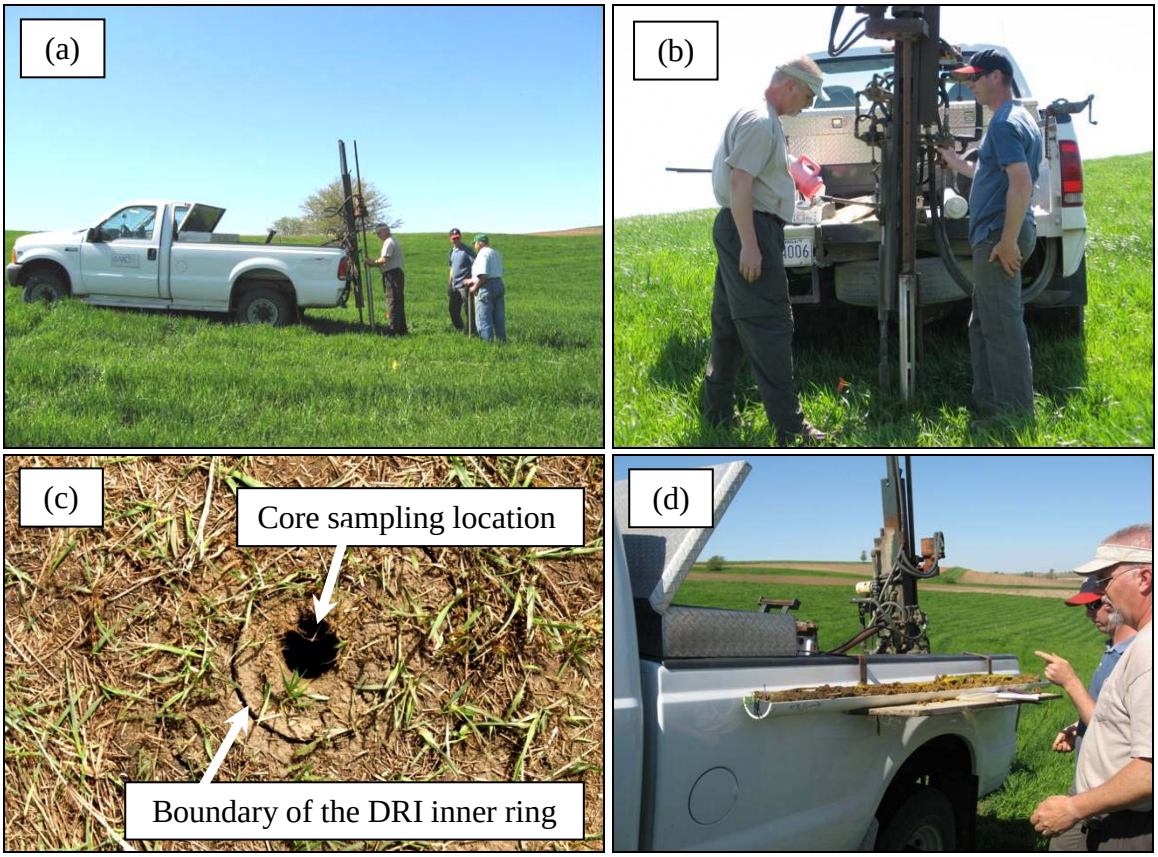

Figure 3.9 Collections of soil core: (a) and (b) Collection of soil cores using the ISU truck mounted Giddings Probe; (c) core sampling location; (d) soil characterization.

Table 3.3 Equations describing the selected statistical mean error criteria.

Statistical mean error criteria	Mathematical expression
The root mean square error	$RMSE = \sqrt{\frac{1}{N}\sum_{i}^{N}(O_i - P_i)^2}$
Akaike Information Criterion	$AIC = N\left(Ln\left(2\pi\sum_{i=1}^{N}(O_i - P_i)^2 / N\right)+1\right)+2k$
The geometric mean error ratio	$GMER = \exp\left(\frac{1}{N}\sum_{i=1}^{N}Ln\left(P_i/O_i\right)\right)$
The geometric standard deviation of the error ratio	$GSDER = \exp\left[\left(\frac{1}{N-1}\sum_{i=1}^{N}\left(Ln\left(P_i/O_i\right)-LnGMER\right)^2\right)^{1/2}\right]$
The range	The minimum and maximum K_{sat} values
The mode	The peak of the K_{sat} distributions

Note: N is sample size, O_i and P_i are the observed and predicted values, respectively, and k is the number of parameters in the models.

Table 3.4 PTFs and watershed models performance.

Criterion*		Mode	Min.	Max.	AIC	RMSE	GMER	GSDER	Total	Ω (%)
PTF	Cosby et al. (1984)	0.8	0.82	0.18	0.85	0.89	0.6	0.71	4.85	69
	Brakensiek et al. (1984)	0.87	0.98	0.42	0.54	0.68	0.36	0.71	4.56	65
	Saxton et al. (1986)	0.85	0.97	0.4	0.51	0.66	0.39	0.72	4.5	64
	Rawls and Brakensiek (1985)	0.32	0.72	0.23	0.96	0.95	0.89	0.86	4.93	70
	Vereecken et al. (1990)	0	0	0.37	0.35	0.47	0	0.14	1.33	19
	Jabro (1992)	0.73	0.94	0.08	0.21	0.15	0.1	0.65	2.86	41
	Dane and Puckett (1994)	0.51	0.68	0.37	0.93	0.93	0.83	0.78	5.03	72
	Campbell and Shiozawa (1994)	0.74	0.91	0.03	0.12	0.1	0.02	0.53	2.45	35
	Risse et al. (1995)	0.85	0.92	0.12	0.33	0.42	0.09	0.5	3.23	46
	Wosten et al. (1999)	0.83	0.91	0.42	0.66	0.81	0.61	0.55	4.79	68
	Rosetta BD - Schaap (1999)	0.59	0.83	0.79	0.79	0.91	0.93	0.76	5.6	**80**
	Rosetta - Schaap (1999)	0.91	0.72	0.17	0.73	0.88	0.67	0.78	4.86	69
WM	KINEROS (Smith et al. 1995)	0.67	0.53	0.18	0.88	0.88	0.58	0.69	4.41	63
	WEPP (Nearing et al. 1996)	0.86	0.98	0.38	0.99	0.97	0.92	0.84	5.94	**85**
	CAESAR (Coulthard et al. 2002)	0.35	0.89	0.28	0.88	0.88	0.58	0.69	4.55	65

*AIC = the Akaike Information Criterion, RMSE = the root mean square error, GMER = the geometric mean error ratio, GSDER = the geometric standard deviation of the error ratio, and Ω = overall performance in percentage.

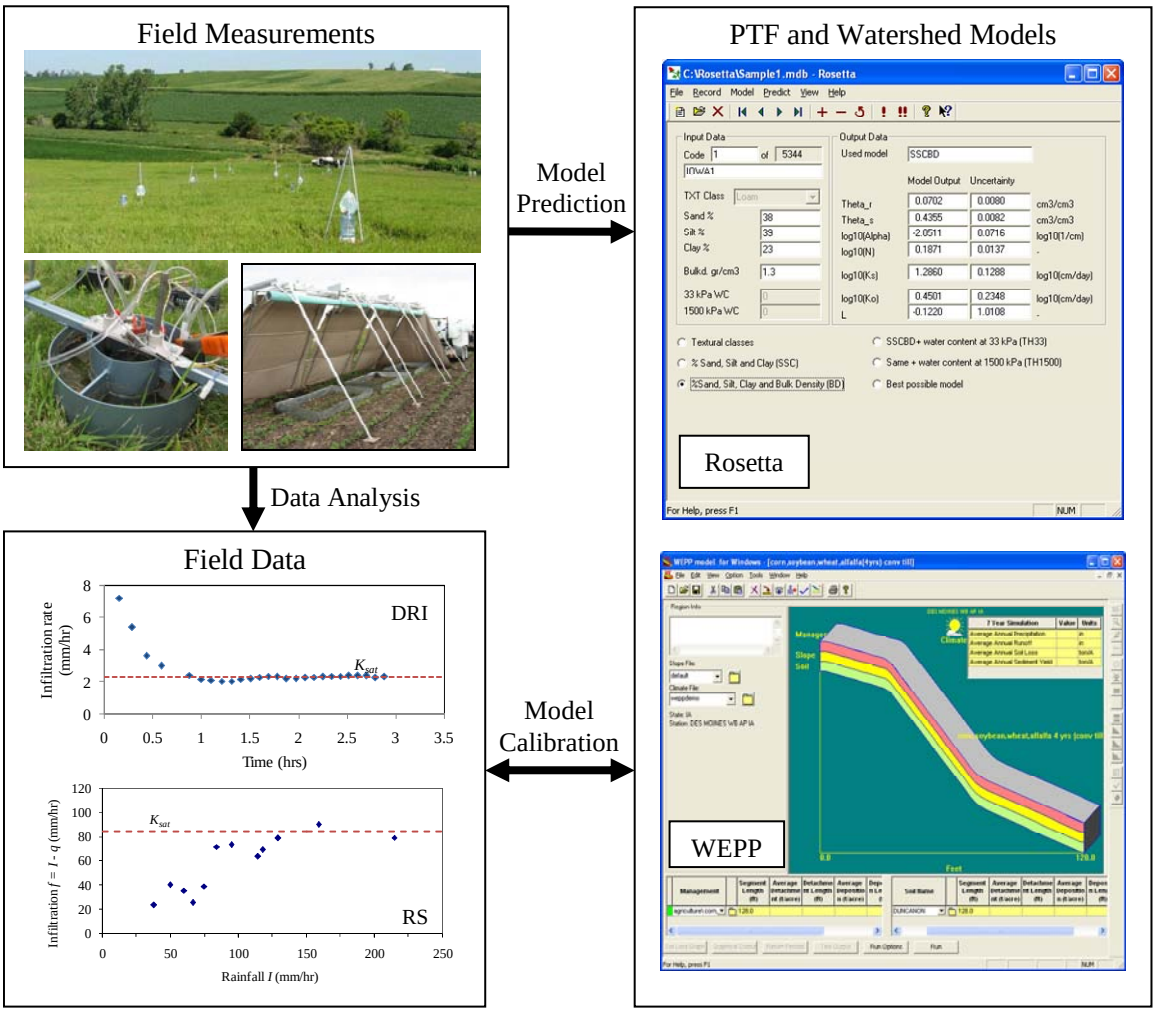

Figure 3.10 Model calibration processes of Rosetta and WEPP.

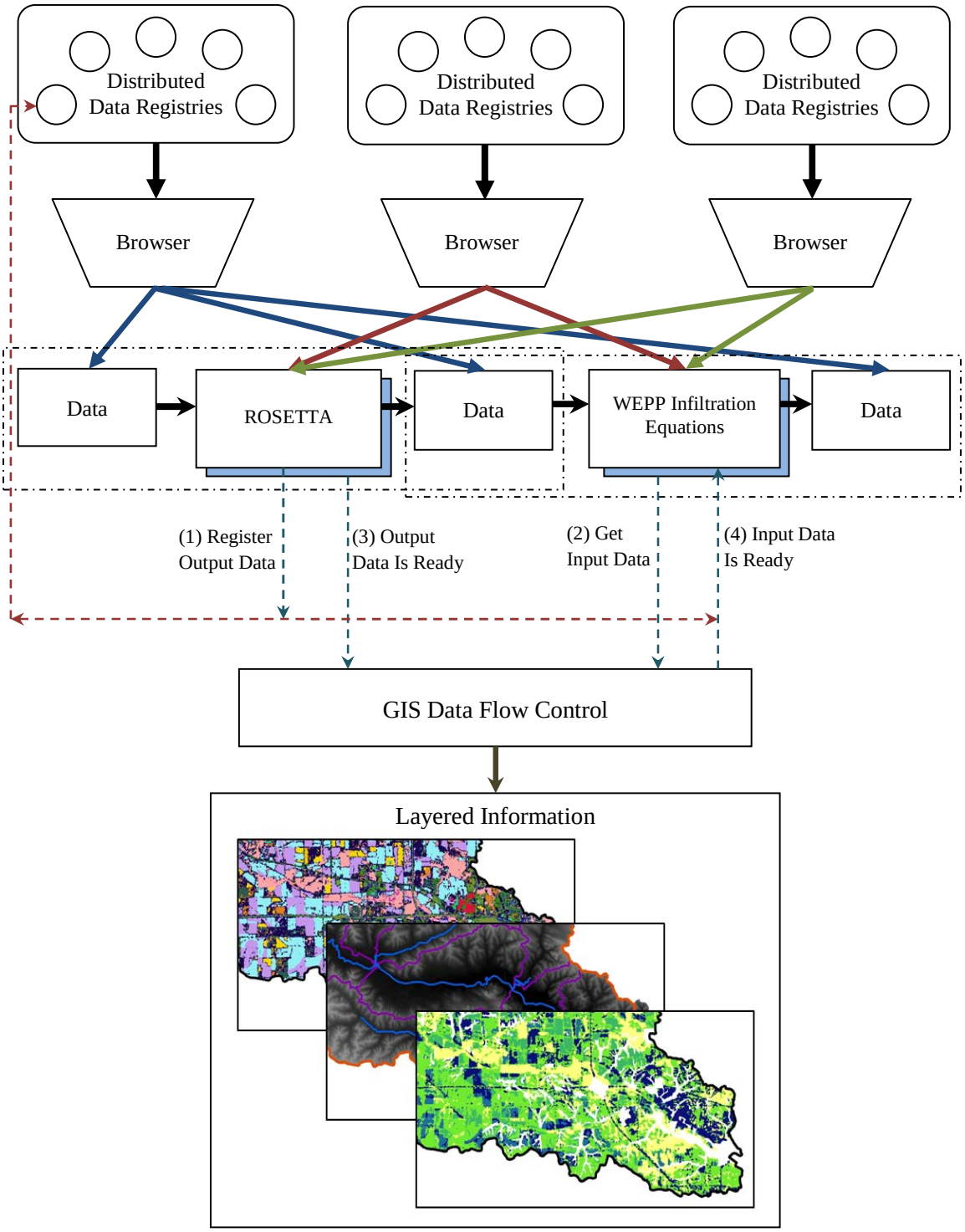

Figure 3.11 An algorithm developed to link the modeling framework components with the layered geospatial data.

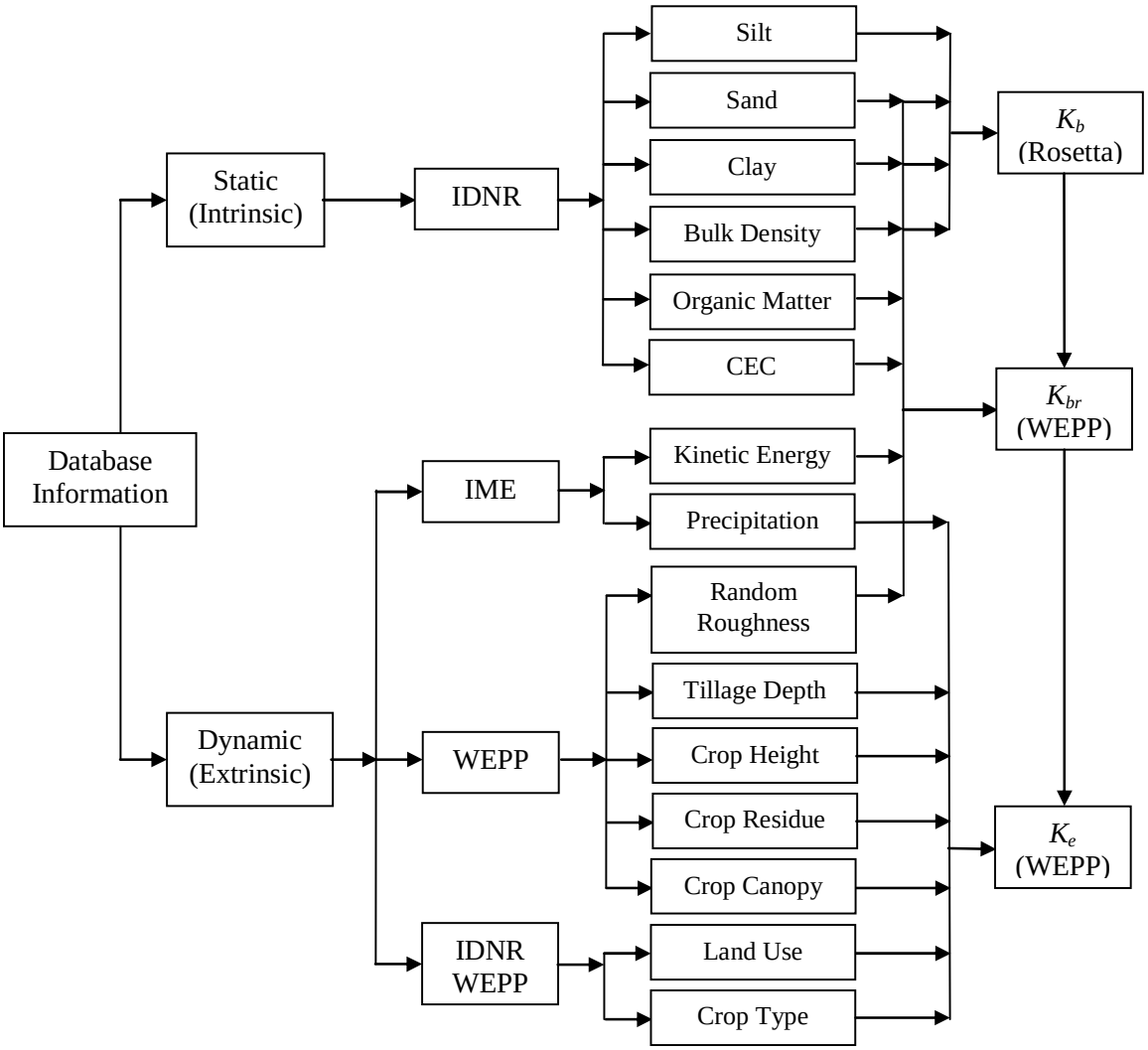

Figure 3.12 Flowchart showing the modeling framework and layered information needed from different sources for K_e estimates.

CHAPTER 4 RESULTS

Saturated hydraulic conductivity (K_{sat}) dynamics was investigated in the Clear Creek Watershed (CCW), IA from the developed physically-based modeling framework. Maps were developed for two different seasons to identify the variability of K_{sat} due to seasonal changes in climate and land use activities. The key variables of the coupled Rosetta-WEPP model were presented in section 4.1, along with the maps and statistical analysis of these variables. K_{sat} maps of CCW for different seasons were presented in section 4.2, followed by statistical analysis of the data to interpret the trends and interrelations among the variables governing K_{sat}.

4.1 Input Variables

The baseline saturated hydraulic conductivity, K_b, was calculated from Rosetta as a function of the soil texture, whereas the bare and effective saturated hydraulic conductivity, K_{br} and K_e, respectively were calculated from WEPP infiltration equation as a function of surface soil properties, precipitation, and vegetation cover (Table 4.1).

The input variables for the models were collected from the databases described in section 3.2.2. The soil information obtained from the SSURGO database was confirmed via the soil cores collected from The Clear Creek Watershed (CCW). About 85% of the soil pedons classified as the same series identified in the published soil survey databases. The land use maps of 2002, which is the latest survey conducted by the Iowa Department of Natural Resources (IDNR), was used as input for the models. There were insignificant changes in the current land uses in the CCW, when compared to the IDNR maps of 2002. The extensive management practices database of the WEPP model was used to estimate the random roughness based on the IDNR inventory.

The rainfall radar data obtained from the IEM was also compared to the tipping bucket data from different stations of the National Climate Data Center (NCDC) in the

CCW. The deviation between the radar and tipping bucket data was less than 10%. Table 4.2 provides the ranges of the input variables used to calculate K_b, K_{br}, and K_e.

Figures 4.1a shows the land use map of 2002 for The Clear Creek Watershed (CCW) obtained from the IDNR. It can be clearly seen that main crops are corn and soybeans, which cover about 50% of the agricultural activities in the CCW (Figure 4.1b). Ungrazed grasslands cover about 23% of the area of CCW. Ungrazed grasslands include rural roads, ditches, grassed waterways, tracts of grasses that are unmanaged, and some grassland/forest edge areas. The remainders of CCW (25%) are forests, planted grasslands, paved roads, and residential and commercial areas (Figure 4.1b).

The total effective cover (C_{TE}) was calculated from the vegetation and management practices databases of WEPP. Because the total effective cover is a function of the canopy and residue cover components, it changes during the life cycle of the crops and hence with season. Figures 4.2a and 4.2b show C_{TE} in the CCW for the months of October, 2007 (before harvesting) and April, 2008 (before planting), respectively. These two seasons were selected to demonstrate the effects of crop leaf intensity and residue cover on C_{TE}. Both maps show higher values, of about 0.95, for C_{TE} in the north-central and southeastern parts of CCW. The north-central part is mainly comprised of forest areas, whereas the southeastern part is mainly comprised of urbanized areas involving the city of Coralville at the eastern boundary of the watershed. Therefore, these areas have insignificant change in C_{TE} values due to seasonal differences. On the contrary, the ungrazed grassland areas show significant changes in C_{TE} values from one season to another. It was on average 0.9 for the month of October, and 0.7 for the month of April.

When comparing the C_{TE} values, where the corn and soybean fields were located within the CCW (see figure 4.1a), it is clear that the corn fields had higher C_{TE} values than soybean fields, which was expected due to the different characteristics of the two crops. Corn and soybeans had average C_{TE} values of 0.75 and 0.37, respectively. For the two crops, however, there were no significant changes in the C_{TE} values of each crop

for the two selected months, because C_{TE} is calculated as the sum of the residue and canopy covers. In the month of October, the fields have intense canopy cover due to the physiological maturity of the corn but very low residue cover. In contrary, in the month of April, the fields have almost no canopy cover but high residue cover from the last harvest.

Figure 4.3 shows the histograms of C_{TE} for the two months. The arithmetic (μ_a), geometric (μ_g), and harmonic (μ_g) mean values as well as the arithmetic (σ_a) and geometric (σ_g) standard deviations are given on the figures. The figures show also the median (m). The month of October shows higher values of C_{TE} than the month of April, which indicates that the canopy cover component has larger impacts on the calculated C_{TE} values than the residue cover component. The zero values on the histograms refer to the water bodies, such as ponds and lakes. The relatively large values of standard deviations are attributed to the land use diversity in the CCW, which include forest, agricultural, grasslands, and urbanized areas.

Figures 4.4 and 4.5 show representative maps for rainfall at the end of the fall and spring seasons in the CCW. Figures 4.4a and 4.4b show maps of the rainfall cumulative kinetic energy (E_a) since last tillage for the fall and spring seasons, respectively. The maps show higher E_a for fall season compared to the spring; however, both seasons show higher E_a values at the western part than eastern part of CCW.

Because K_e is a function of vegetation cover (canopy and residue) and single storm events, the days of the highest rainfall events in October, 2007 (before harvesting) and April, 2008 (before planting) were selected to demonstrate the maximum effect of rainfall on K_{sat}. Figure 4.5 shows the rainfall depth (P) maps for these two days. The maps show higher rainfall depth for the single event of October 17th, 2007 compared to that of April 18th, 2008. The October event showed higher P values at the central part of the watershed, while the April event showed higher P values at the western part.

Statistical analysis of the rainfall data used to develop the maps shown in Figures 4.4 and 4.5 are given in Figure 4.6 and 4.7, respectively. Figure 4.6a and 4.6b show the histograms of E_a since last tillage for the fall and spring seasons, respectively. Figure 4.6 shows that the distributions of E_a values are more scattered in the fall compared to the spring. Figure 4.7 shows the histograms of P for the two single events, with a bimodal distribution on the April 18th, 2008 event. Nonetheless, the small standard deviations and the insignificant differences between the calculated mean values indicated that the rainfall was fairly uniform over the watershed which was expected for the size of the CCW (less than 300 km^2). These near uniformity distributions were also apparent in the developed rainfall maps.

4.2 K_{sat} Variability in the Clear Creek Watershed

This modeling framework facilitated the prediction of K_{sat} variability in the Clear Creek Watershed (CCW) due to seasonal changes in climate and land use activities. Maps of baseline (K_b), bare (K_{br}), and effective (K_e) saturated hydraulic conductivity were presented in this section for the two seasons along with statistical analysis of the data used in developing the maps. Figure 4.8 shows the baseline saturated hydraulic conductivity (K_b) for the CCW calculated from Rosetta as a function of soil textures and bulk density. Except for the northeastern area of the watershed, the map shows, in general, higher K_b values on the northern part of the CCW compared to the southern part. This was attributed to differences in the soil textures of the two parts. The soil texture of the northern part of the CCW had lower percentage of clay compared to the southern part, which had higher percentage of clay in its soil composition. The average clay percentages in the soils of the northern and southern parts of the CCW were 11% and 23%, respectively. The percentage of clay in the northern part soils agreed with the

percentage of clay found in the soil core samples collected from the South Amana Subwatershed, which is located on the northwestern part of the CCW.

Figure 4.9 shows bare saturated hydraulic conductivity (K_{br}) maps of CCW for the months of October, 2007 and April, 2008, respectively. K_{br} was calculated from WEPP as a function of crust factor, soil stability factor, random roughness (RR_t), and cumulative rainfall kinetic energy (E_a). The last two are the dynamic parameters accounting for the changes in the management practices and climate conditions, respectively through the year.

The RR_t for the two selected months was calculated from WEPP. The months of October and April corresponded to the conditions before harvesting and before planting, respectively. Both months have an average RR_t value of 0.01 m, which corresponded to the minimal land surface disturbance just before tillage. The after tillage months were avoided because $K_{br} = K_b$, which will not allow for the examining of the effects of the second dynamic parameter E_a. The cumulative rainfall kinetic energy, E_a, was calculated for the month of October, 2007 from the precipitation data of May to October, 2007 and for the month of April, 2008 from the precipitation data of November, 2007 to April, 2008. The month of April had an overall higher K_{br} values than the month of October, because K_{br} is inversely proportional to E_a and the winter and spring seasons in Iowa are characterized by lower precipitation compared to the summer and fall seasons. The inverse proportional relationship between K_{br} and E_a can be physically explained by the amount of eroded soils that form the surface crust layer. For a specific soil, the higher the precipitation, the larger the amount of eroded soils, and hence the thickness of the formed crust layer. This will reduce the permeability of soil, and hence reduce the value of K_{br}. A similar finding has been reported by Eigel et al. (1983).

The effective saturated hydraulic conductivity (K_e) is a function of the total effective cover (C_{TE}) which includes factors such vegation cover (canopy and residue), lakes, and urbanized areas. It has also an additional factor that accounts for the effects of

single storm events. Therefore, K_e is the most dynamic among the three expressions of saturated hydraulic conductivity (K_b, K_{br}, and K_e). The time scale for the change of K_e can be as small as few hours, whereas the time scale of K_{br} dynamics is a season (Abaci and Papanicolaou 2009). The time scale of K_b dynamics, on the other hand, can be of order of 10 years (Papanicolaou et al. 2009).

The effect of land cover only on K_e was first examined without considering any single storm event. Figure 4.10 shows the maps of the K_e in the CCW without the rainfall effect, denoted as $K_{e\text{-}nr}$, for the months of October and April, respectively. Both maps show lower values of $K_{e\text{-}nr}$ in the north-central and southeastern parts of CCW, which reflect the high values of total effective cover (C_{TE}) shown on Figure 4.2. These trends agree with the land uses of these parts of the watershed, which are mainly comprised of forest and urbanized areas involving the city of Coralville at the eastern boundary of the watershed. Thus, there were no significant changes in $K_{e\text{-}nr}$ values at these areas due to seasonal differences.

When comparing the $K_{e\text{-}nr}$ values, where the corn and soybean fields were located within the CCW (see figure 4.1a), it is clear that the corn fields had lower $K_{e\text{-}nr}$ values than soybean fields, a trend that has been mostly attributed to the different associated management practices and degree of soil disturbance for corn and soybean (e.g., primary and secondary tillages) (Abaci and Papanicolaou, 2009). For the two crops, however, there were no significant changes in the $K_{e\text{-}nr}$ values of each crop for the two selected months. On the contrary, ungrazed grassland areas show significant changes in $K_{e\text{-}nr}$ values from one season to another. The differences in $K_{e\text{-}nr}$ values of the crops and ungrazed grassland areas were explained by the differences in the total effective cover (C_{TE}) characteristics, which were explained in section 4.1.

K_e maps with the additional term that accounts for the effects of single storm events are shown in Figure 4.11. The maps are plotted for the days of the highest rainfall events in October, 2007 and April, 2008 to demonstrate the maximum effect of rainfall

on K_e. For the October event, the K_e values were higher at the central part of the watershed, while for the April event the K_e values were higher at the western part. These were attributed the rainfall distribution over the watersheds during these two days (see Figure 4.5). Because K_e is linearly proportional to rainfall depth and the October event had higher precipitation than the April event, overall the maps show higher K_e for the single storm event of October 17th, 2007 compared to that of April 18th, 2008. The proportional relationship between K_e and rainfall depth can be explained by the fact that the higher the precipitation the more likelihood that the protective crust layer will be broken, and hence allowing for higher infiltration rates. Wischmeier (1966) has shown that positive correlation exists between K_e and rainfall depth.

A comparison of the relative magnitudes of K_b, K_{br}, $K_{e\text{-}nr}$, and K_e for the months of October and April is given in Figures 4.13. The geometric mean (μ_g) or median (m) are more representative for the distributions of the saturated hydraulic conductivity due to its wide range. Both months show higher median values for K_b (K_b is the same for both months because it is a function of soil texture only) when compared to other saturated hydraulic conductivity values. The histograms of K_{br} emphasize the important roles of cumulative rainfall kinetic energy (E_a) and management practices on saturated hydraulic conductivity, noted also by Rawls and Brakensiek (1989).

For the month of October, the upper limit of K_{br}, which is about 6.0 mm/hr with 90% confidence limit, represents nearly the lower limit of K_b under the same confidence limit. For the month of April, E_a was lower than the month of October; therefore, the distribution of K_{br} was almost the same as K_b with a reduction of about 2 mm/hr in the median value. Nonetheless, the K_{br} histograms, in general, show a more uniform distribution patterns compared to K_b. The histograms of $K_{e\text{-}nr}$ show considerable reduction in their values when compared to K_b, which indicate that the total effective cover C_{TE} is one of the predominant factors that affect saturated hydraulic conductivity. The histograms of $K_{e\text{-}nr}$ show a positively skewed distribution for both months. The

histograms of K_e show an increase in the saturated hydraulic conductivity when compared to $K_{e\text{-}nr}$, with a near symmetric distribution. The median values increased about 5 and 3 mm/hr for the months of October and April, respectively. This increase in K_e shows the important role of single storm events in estimating the saturated hydraulic conductivity (Wischmeier 1966).

The maps and histograms shown in Figures 4.9 to 4.12 were normalized by the baseline hydraulic conductivity, K_b. The ratios of K_{br}, $K_{e\text{-}nr}$, and K_e to K_b for the month of October are given in Figures 4.13. Figure 4.13a shows the ratio K_{br}/K_b, which ranges between 0.47 and 0.72. For most of the areas within watershed, a 30% reduction in K_b was observed due to changes in management practices and climate conditions through the season. This was also confirmed from the histogram, which shows a median of 0.67. As can be seen from the histogram, K_{br} is always smaller than K_b. The baseline hydraulic conductivity, K_b, is the upper limit of K_{br}, which can be approached only immediately after tillage.

Figure 4.13b shows the ratio $K_{e\text{-}nr}/K_b$, which ranges between 0.0 and 0.71. For most of the areas within watershed, a 50% reduction in K_b was observed due to changes in vegetation cover through the season. It can be seen from the histogram that $K_{e\text{-}nr}$ is always smaller than K_b, with a median of 0.14.

Lastly, figure 4.13c shows the ratio K_e/K_b, which ranges between 0.46 and 1.59. As can be seen from the histogram, K_e can be either smaller or larger than K_b, with a median of 0.75. Within the watershed, the K_e values which were larger than K_b were less than 5%. This can be explained by the effects of rainfall on the porous structure of the surface soil at these locations.

Similar trends for these ratios were also observed for the month of April. The maps and histograms for the month of April are provided as Figure D1 in Appendix D.

Table 4.1 Inputs of K_b, K_{br} and K_e.

	K_b (Rosetta)	K_{br} (WEPP)	K_e (WEPP)
Inputs	% Sand	K_b	K_b
	% Silt	Crust factor	K_{br}
	% Clay	Soil Stability factor	Residue cover
	Bulk density	Random roughness	Canopy cover
		Cumulative rainfall kinetic energy	Precipitation

Table 4.2 Ranges of the input variables for CCW.

K_{sat}	Input parameters	Unit	Maximum	Minimum
K_b	% Sand (*Sa*)	Fraction	86	3
	% Clay (*Cl*)	Fraction	36	6
	Bulk density (*BD*)	Kg/m^3	1.53	1.27
K_{br}	K_b	mm/h	83.6	2.5
	Cation Exchange Capacity (*CEC*)	*meq/100g*	39	0
	Crust factor (*CF*)	dimensionless	0.5378	0.4324
	Soil stability factor (*C*)	m^2/J	0.00786	0.0001
	Random roughness (RR_t)	m	0.04	0.01
	Cumulative Rainfall Kinetic Energy-May, 2007 ~ October, 2007 (E_a)	kJ/m^2	13.2	9.8
	Cumulative Rainfall Kinetic Energy-November, 2007 ~ April, 2008 (E_a)	kJ/m^2	6.1	4.6
K_e	Precipitation- 10/17/2007 (*P*)	mm	48.8	36.6
	Precipitation- 4/18/2008 (*P*)	mm	34.8	20.8
	Total effective cover-October (C_{TE})	Fraction	1	0
	Total effective cover-April (C_{TE})	Fraction	1	0
	K_{br} – October, 2007	mm/h	42.8	1.3
	K_{br} – April, 2008	mm/h	42.8	1.3

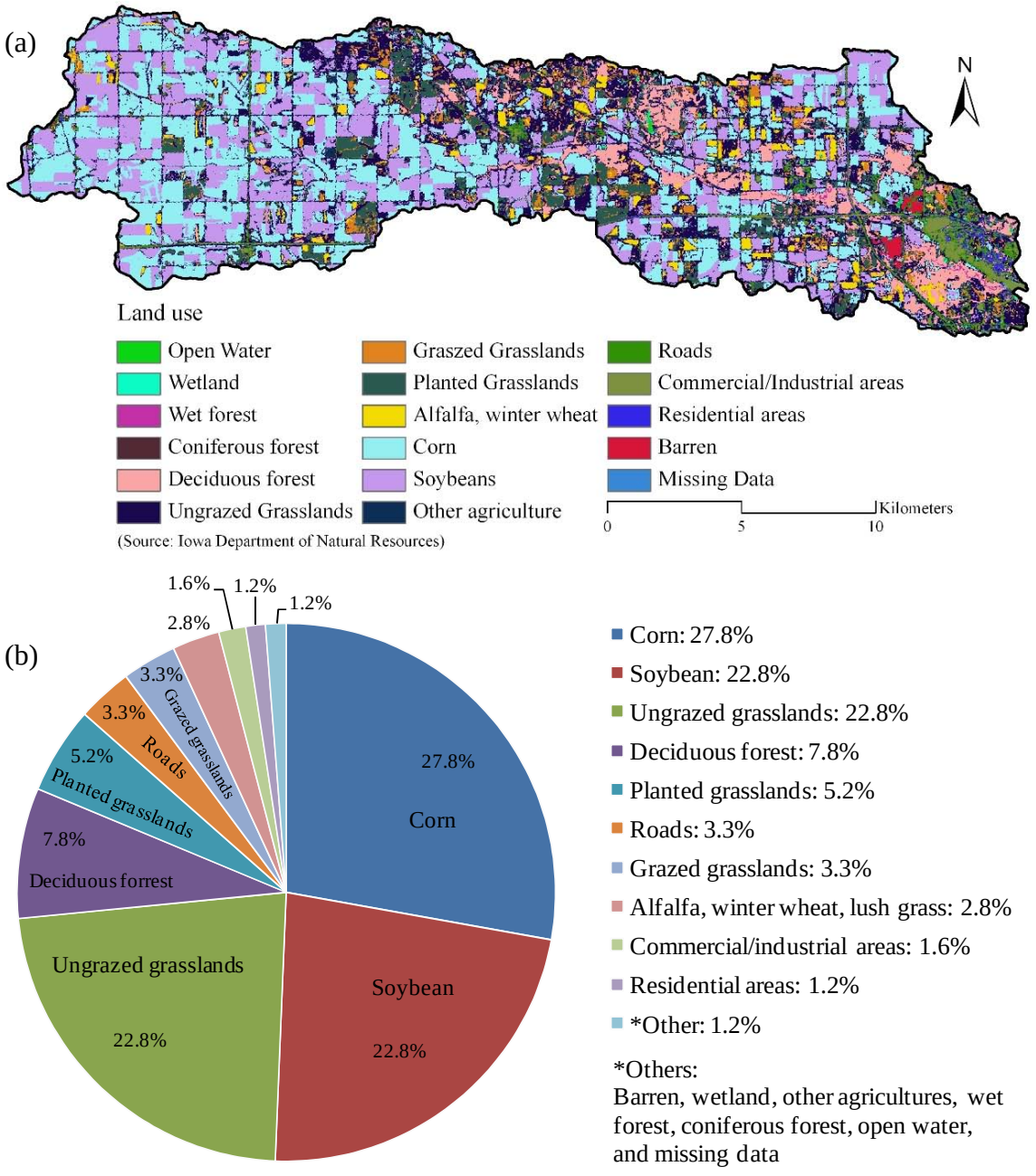

Figure 4.1 Land uses in The Clear Creek Watershed, IA: (a) map; (b) pie chart.

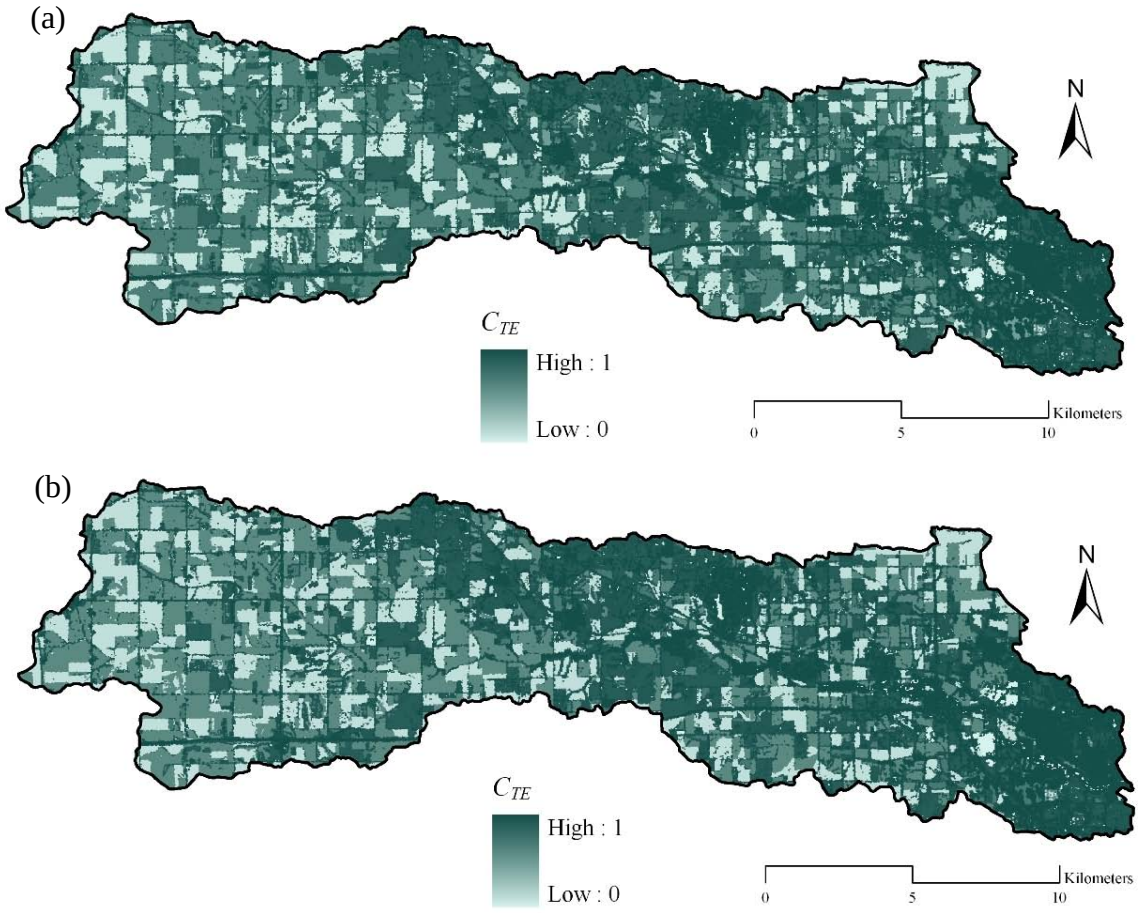

Figure 4.2 Total effective cover C_{TE} (a) in October, 2007; (b) in April, 2008 in the CCW, IA.

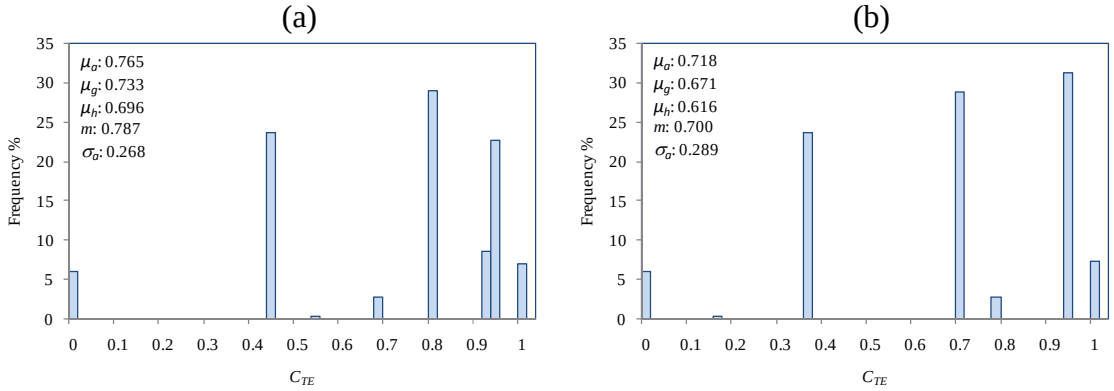

Figure 4.3 Histograms of C_{TE} (a) in October, 2007; (b) in April, 2008 in the CCW, IA.

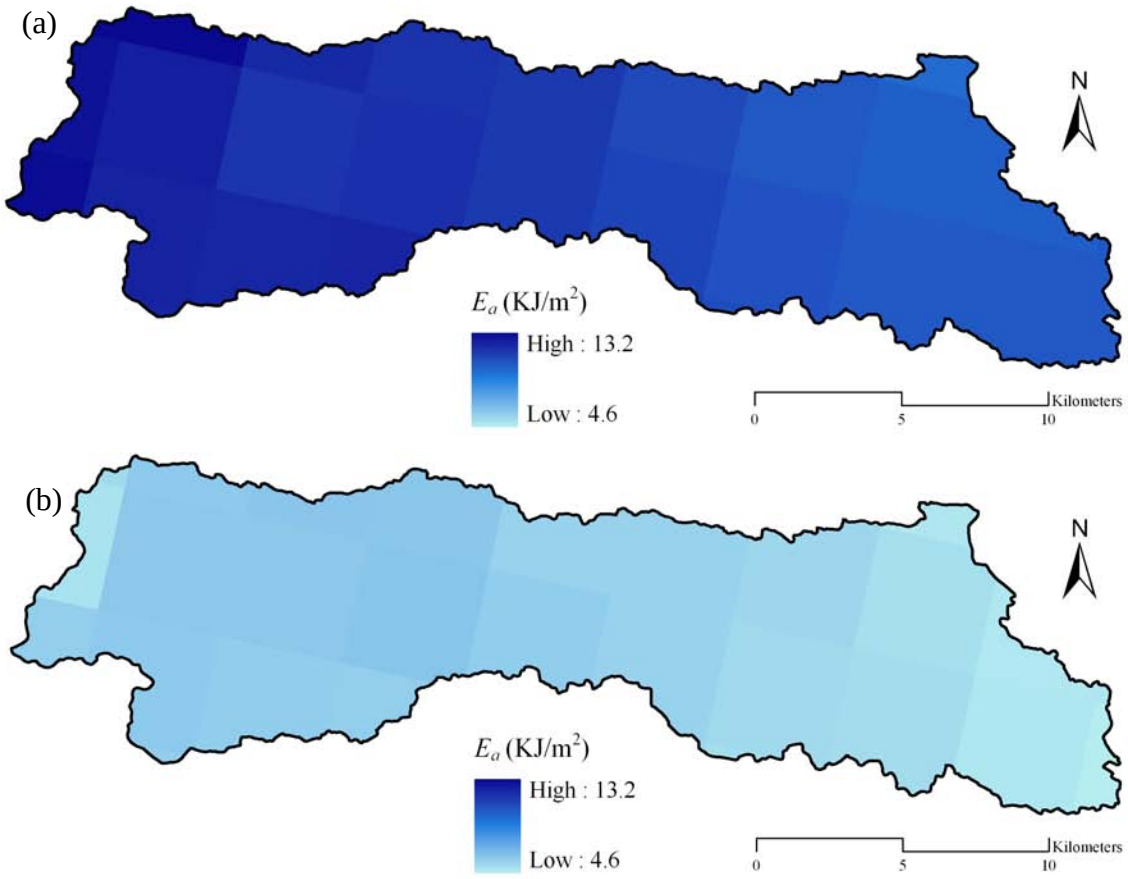

Figure 4.4 Cumulative rainfall kinetic energy distribution (a) from May, 2007 to October, 2007; (b) from November, 2007 to April, 2008 in the CCW, IA.

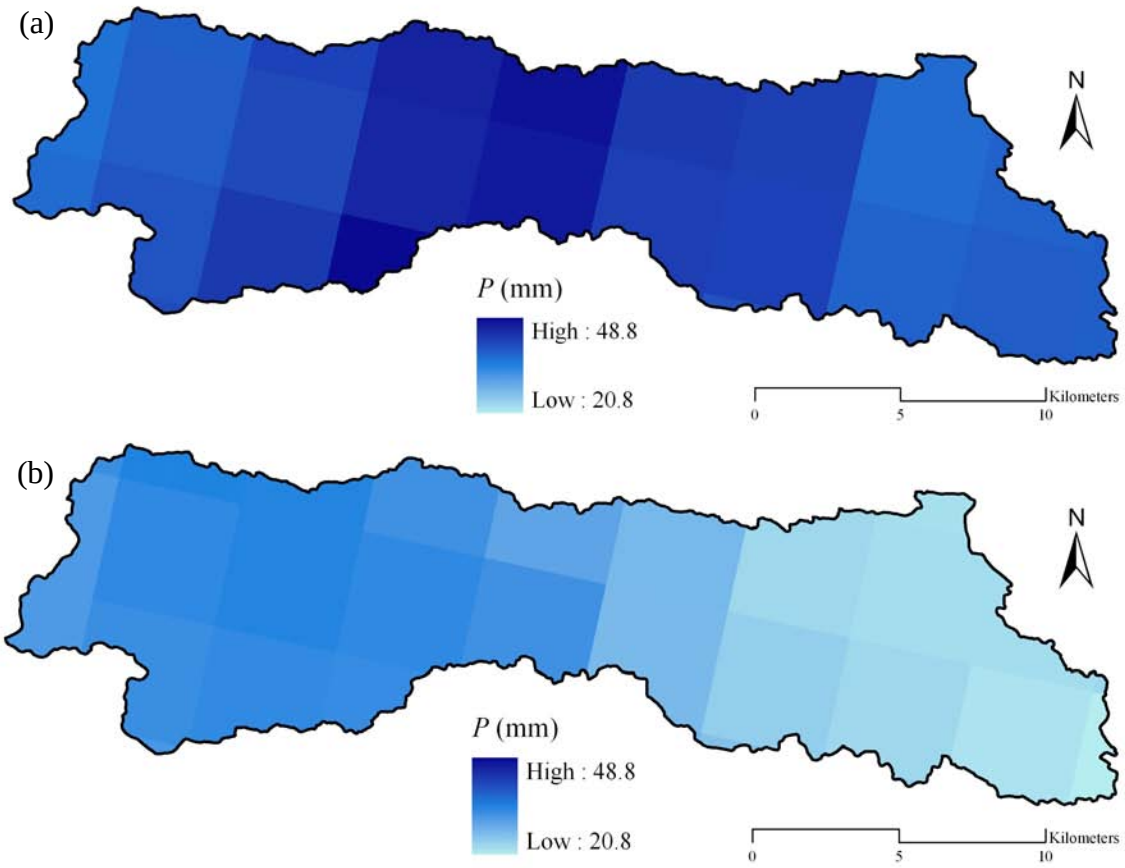

Figure 4.5 Rainfall depth distribution on: (a) October 17th, 2007; (b) April 18th, 2008 in the CCW, IA.

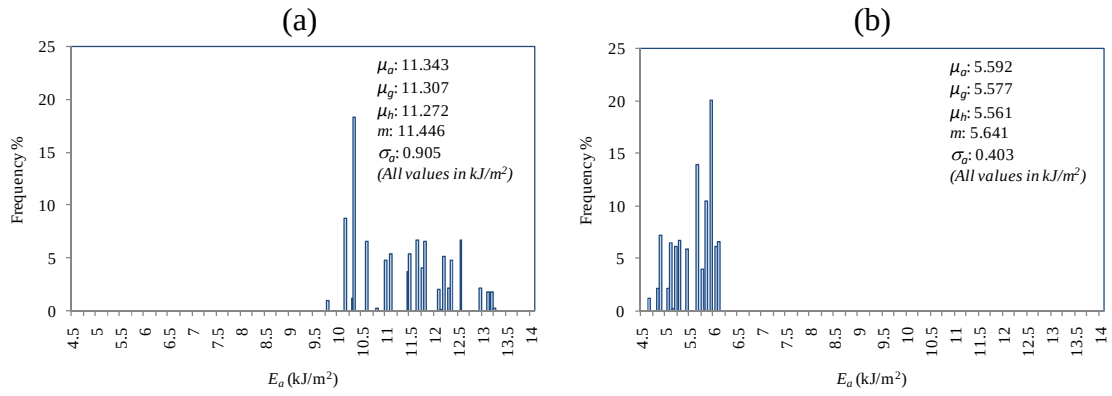

Figure 4.6 Cumulative rainfall kinetic energy for (a) May to October, 2007; (b) November, 2007 to April, 2008 in the CCW, IA.

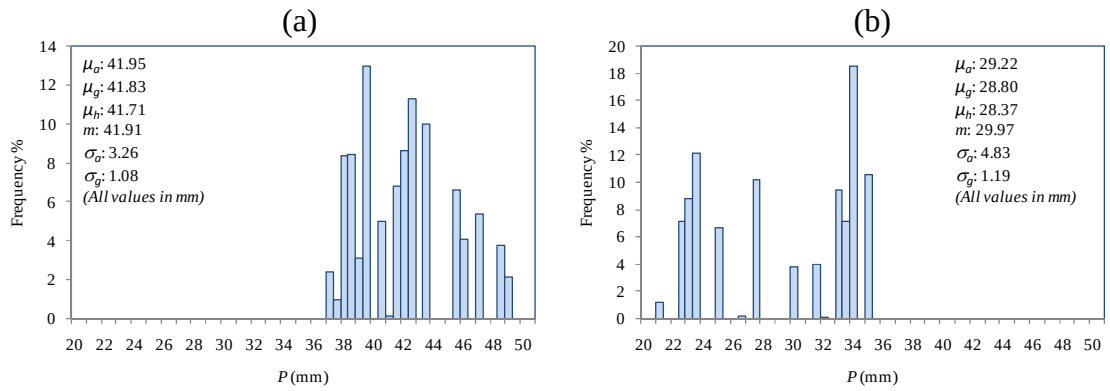

Figure 4.7 Single storm event on (a) October 17th, 2007; (b) April 18th, 2008 in the CCW, IA.

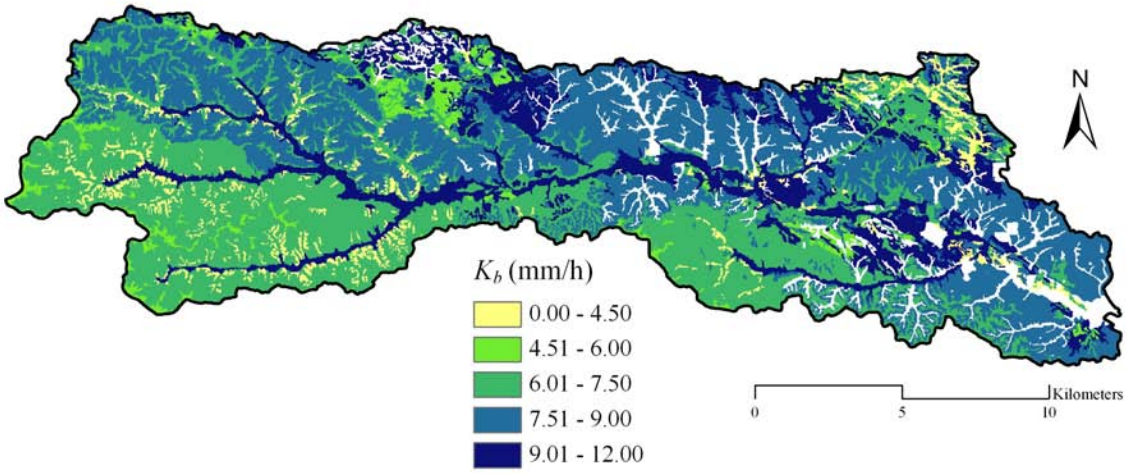

Figure 4.8 K_b in the CCW, IA.

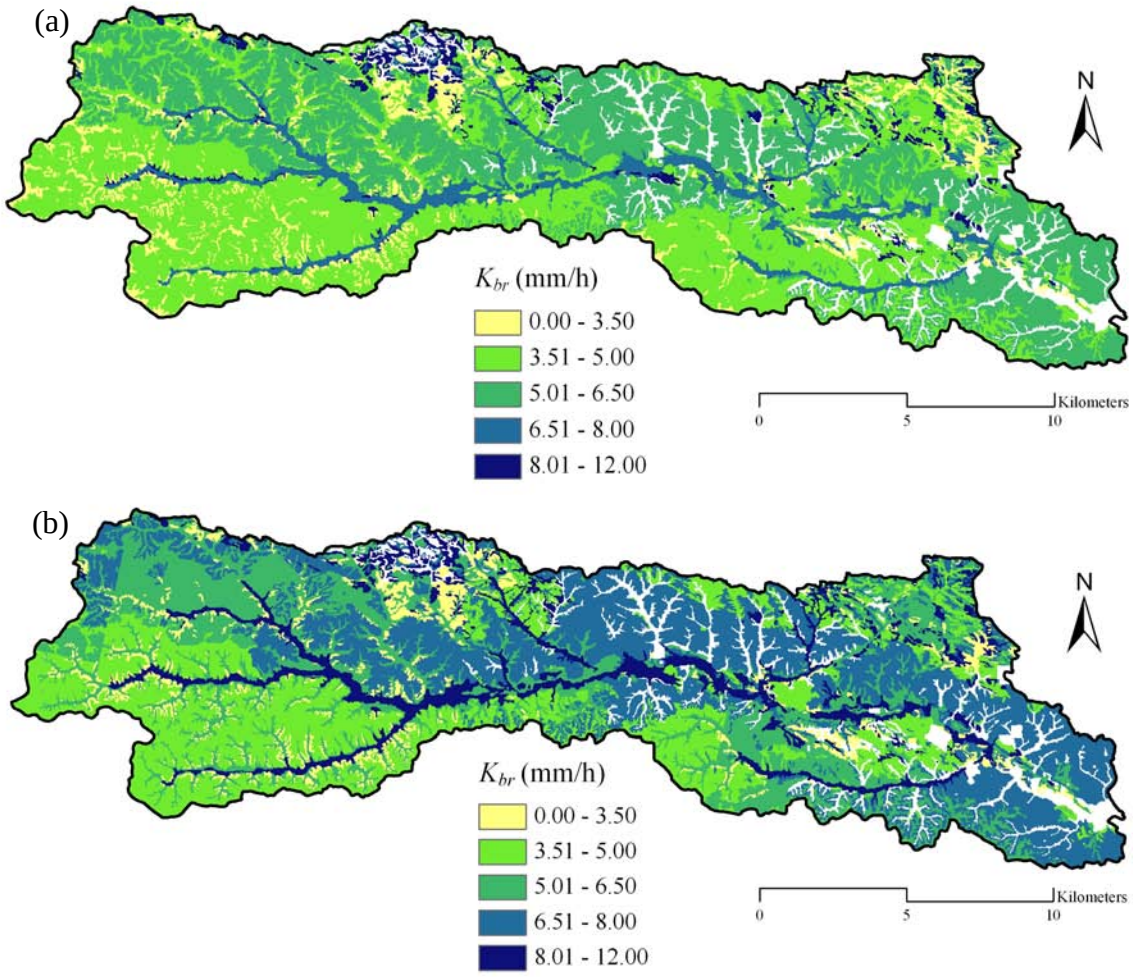

Figure 4.9 K_{br} in: (a) October, 2007; (b) April, 2008 in the CCW, IA.

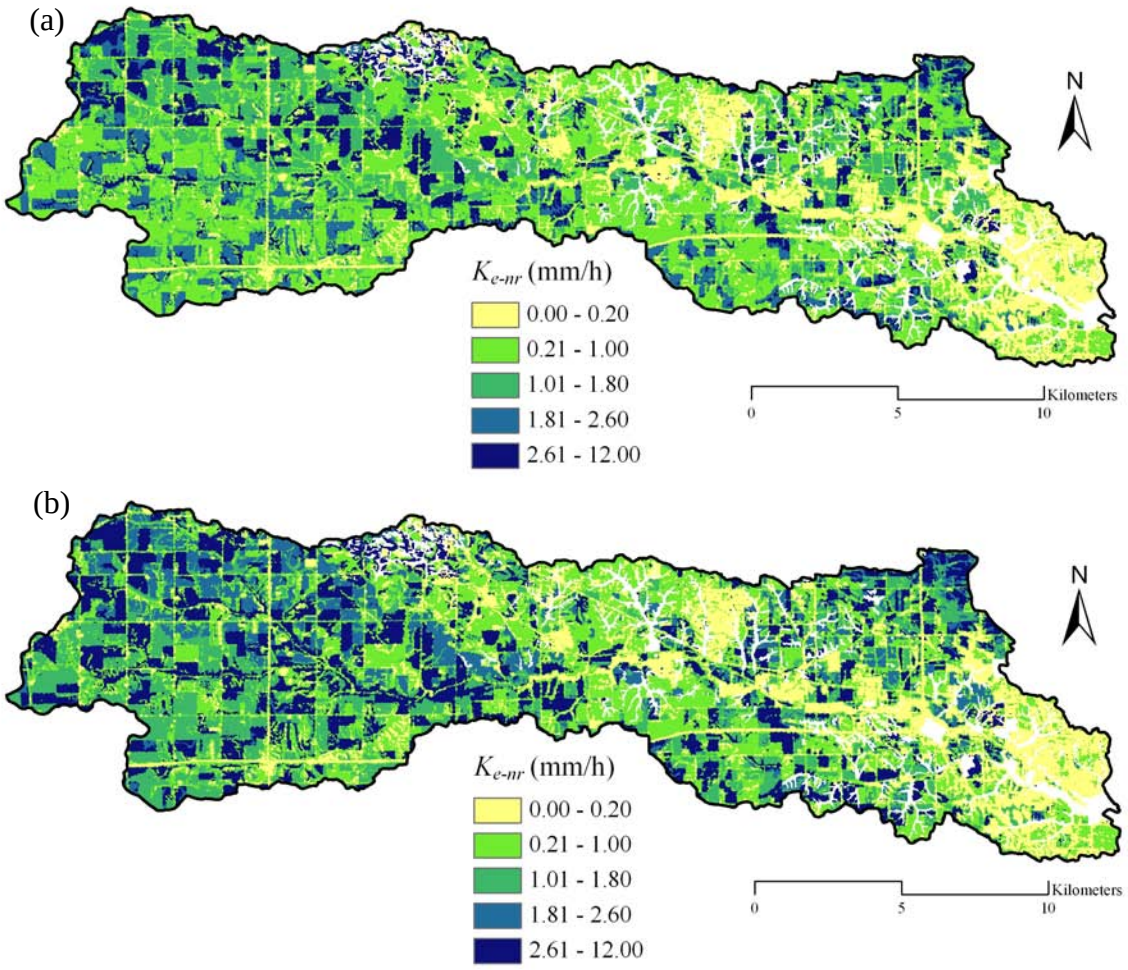

Figure 4.10 $K_{e\text{-}nr}$ in: (a) October, 2007; (b) April, 2008 in the CCW, IA.

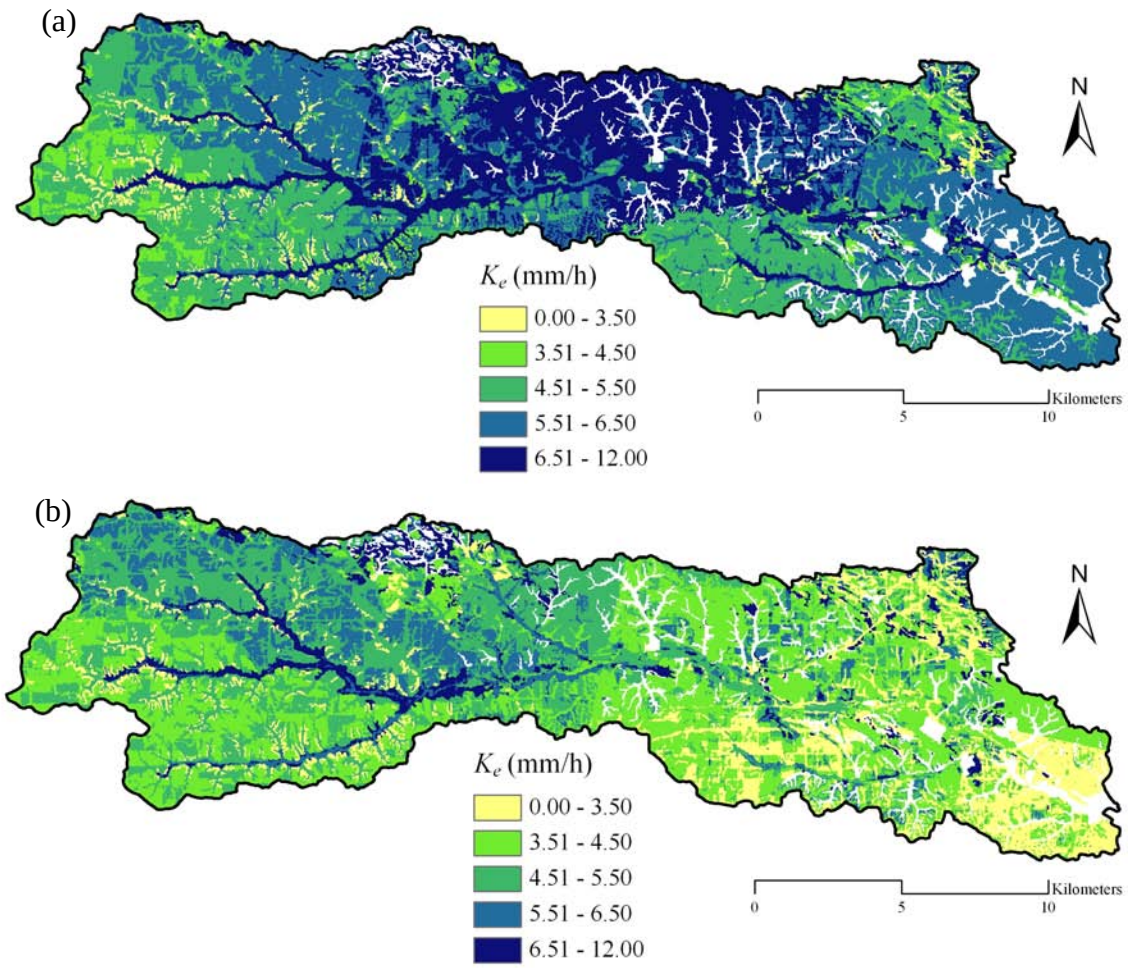

Figure 4.11 K_e on: (a) October 17th, 2007; (b) April 18th, 2008 in the CCW, IA.

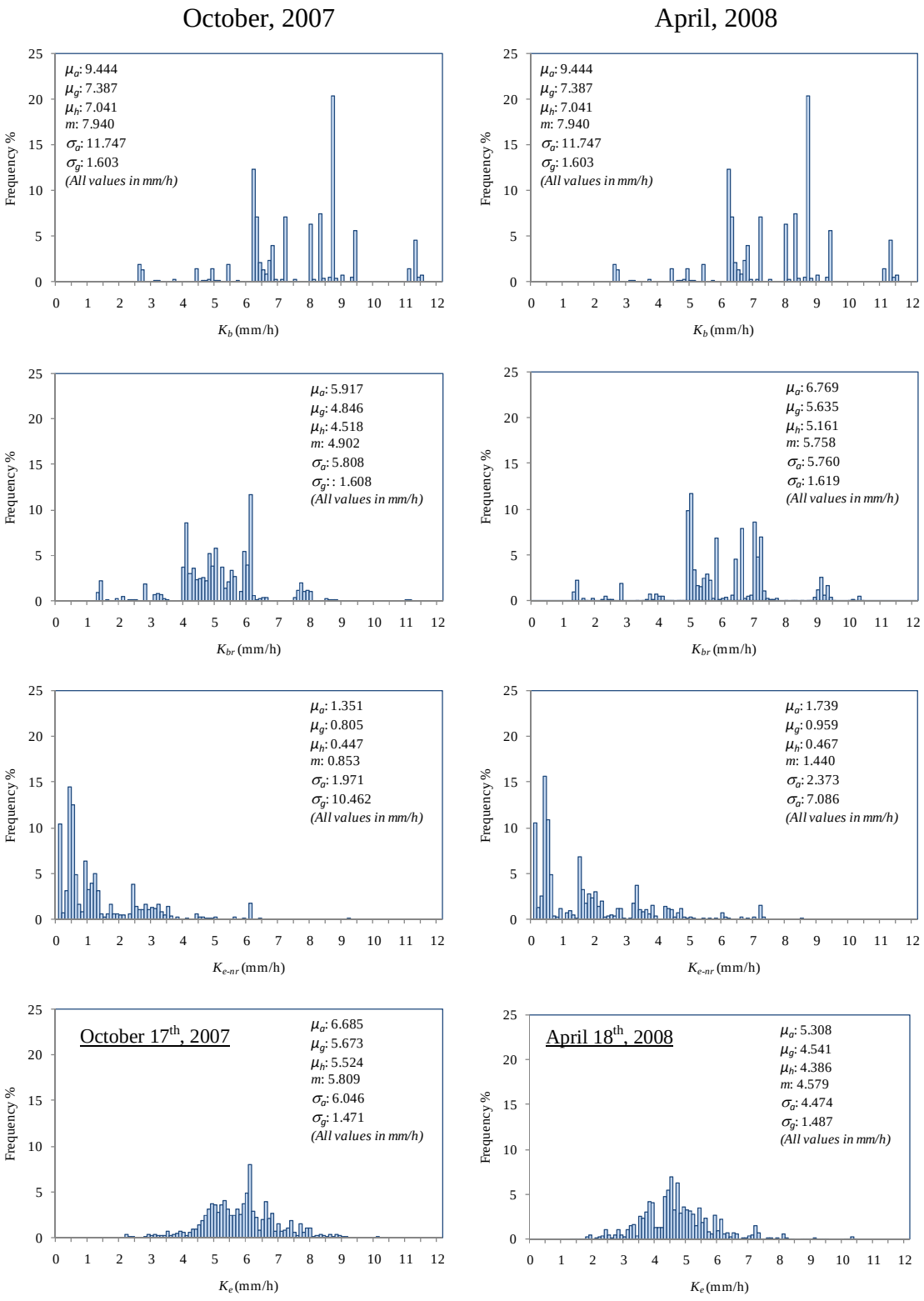

Figure 4.12 Summaries of the K_b, K_{br}, $K_{e\text{-}nr}$, and K_e histograms.

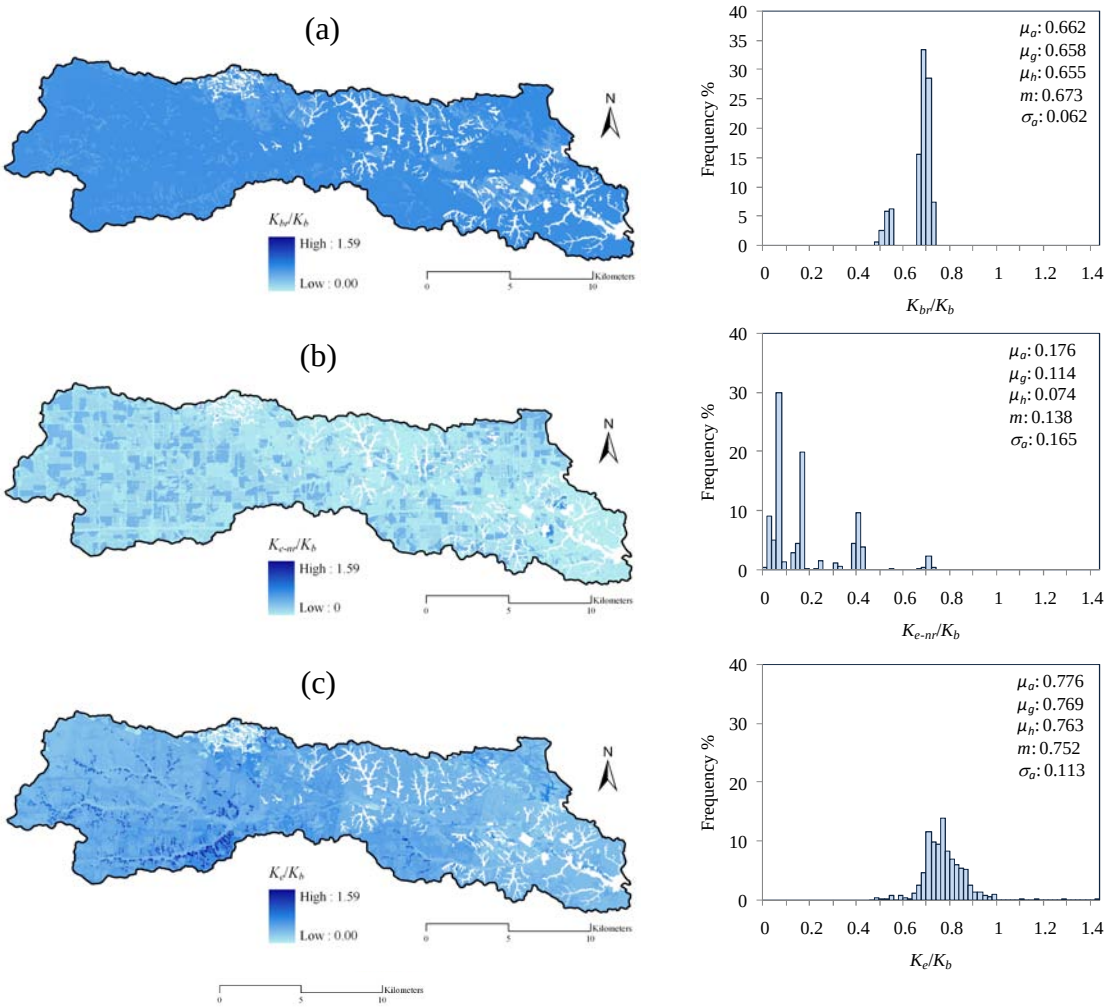

Figure 4.13 Ratios of K_{br}, $K_{e\text{-}nr}$, and K_e to K_b for the month of October in the CCW, IA.

CHAPTER 5 CONCLUSIONS AND SUMMARY

A physically-based, modeling framework within which different geographic, climatic, and land use data can be incorporated was developed to predict K_{sat} dynamics in the Clear Creek Watershed (CCW), IA. The modeling framework integrated selected pedotransfer functions (PTFs) and watershed models with geospatial tools. A number of PTFs and watershed models were examined to select the appropriate models that represent the study site conditions. Models selection was based on statistical measures of the models' errors compared to the field measurements conducted in the CCW. The study has shown that Rosetta and the Water Erosion Prediction Project (WEPP) predictions provided the best agreement to the measured K_{sat} values in the CCW compared to the other tested models. Therefore, Rosetta and WEPP were used to calculate the baseline (K_b) and effective (K_e) saturated hydraulic conductivity, respectively. Rosetta and WEPP were integrated with the Geographic Information System (GIS) tools by developing a program that facilitates the compilation of different geographically distributed data from registries of the data sources and computational resources of the models into GIS platform. The modeling framework allowed for visualization of the data in forms of geospatial maps and prediction of K_{sat} variability in the CCW due to the seasonal changes in climate and land use activities. Two seasons were selected to demonstrate K_{sat} dynamics; specifically, the months of October and April, which corresponded to the before harvesting and before planting conditions, respectively. The following points summarize the findings related to K_b, K_{br}, and K_e:

(1) Baseline saturated hydraulic conductivity (K_b)

K_b was calculated from Rosetta as a function of soil textures and bulk density. Therefore, it does not change considerably throughout the year. Except for the northeastern area of the watershed, K_b exhibited higher values on the northern part of the CCW compared to the southern part, because the soil texture of the northern part of the

CCW had lower percentage of clay compared to the southern part. This was confirmed also from the core samples collected from the CCW.

(2) Bare saturated hydraulic conductivity (K_{br})

The two selected months had an average random roughness value of 0.01 m, which was calculated from WEPP management practice database. This value corresponded to the minimal land surface disturbance just before tillage. The after tillage months were avoided because bare saturated hydraulic conductivity $K_{br} = K_b$, which will not allow for the examining of the effects of cumulative rainfall kinetic energy (E_a). The month of April had an overall higher K_{br} values than the month of October, because K_{br} is inversely proportional to E_a and spring season in Iowa are characterized by lower precipitation compared to the fall season.

(3) Effective saturated hydraulic conductivity (K_e)

The two selected months show insignificant difference in $K_{e\text{-}nr}$ values ($K_{e\text{-}nr}$ defined as K_e that accounts for land cover without considering precipitation) at the north-central and southeastern parts of CCW. The $K_{e\text{-}nr}$ values were also low at these parts of the watershed, which are mainly comprised of forest and urbanized areas involving the city of Coralville. The corn fields showed lower $K_{e\text{-}nr}$ values than soybean fields, however, there were no significant changes in the $K_{e\text{-}nr}$ values of each crop for the two months. On the contrary, ungrazed grassland areas showed significant changes in $K_{e\text{-}nr}$ values from one season to another. The differences in $K_{e\text{-}nr}$ values of the crops and ungrazed grassland areas were due to different characteristics of the plants.

The days of the highest rainfall events in October, 2007 and April, 2008 were selected to demonstrate the maximum effect of rainfall on K_e. For the October event, the K_e values were higher at the central part of the watershed, while for the April event the K_e values were higher at the western part. These were attributed the rainfall distribution over the watersheds during these two days. However, overall K_e was higher for the single storm event of October 17th, 2007 than that of April 18th, 2008, because K_e is linearly

proportional to rainfall depth and the October event had higher precipitation than the April event.

(4) General summary

Statistical analysis of the distributions of K_b, K_{br}, $K_{e\text{-}nr}$, and K_e in the CCW has shown that the geometric mean or median was more representative for the distributions of different saturated hydraulic conductivities due to their wide ranges. Both months show higher median values for K_b, when compared to other saturated hydraulic conductivity values. The K_{br} histograms showed a more uniform distribution patterns compared to K_b. $K_{e\text{-}nr}$ showed considerable reduction in their values when compared to K_b, which demonstrates the important role of land cover. The histograms of $K_{e\text{-}nr}$ show a positively skewed distribution for both months. K_e showed an increase in the saturated hydraulic conductivity when compared to $K_{e\text{-}nr}$, with a near symmetric distribution. This increase in K_e showed the important role of single storm events in estimating the saturated hydraulic conductivity.

The applicability of the pedotransfer function and watershed model used within the developed modeling framework is limited to the investigated watershed and other watersheds in Iowa having similar soils, management practices, and climatic conditions, mostly in eastern Iowa. As the proposed modeling framework was able to successfully capture the spatial and temporal variability of K_{sat} at the watershed scale, it would be advisable to repeat this study in different counties or even in other parts of the country, where arid or semi-arid conditions are ubiquitous, using different pedotransfer functions and watershed models. This can contribute to the development of ratings for many of the soil interpretations incorporated into the National Cooperative Soil Survey (NCSS) and update the K_{sat} data stored in the National Soil Information System (NASIS) database.

REFERENCES

1. Amoozegar, A. "A Compact Constant-Head Permeameter for Measuring Saturated Hydraulic Conductivity of the Vadose Zone." *Soil Science Society of America Journal* 53, no. 5 (1989): 1356-1361.

2. Amoozegar, A., and G.V. Wilson. "Method for measuring hydraulic conductivity and drainable porosity." *Agricultural drainage, agronomy monograph*, 1999: 1149–1205.

3. Ascough, J.C., M.A. Nearing, D.C. Flanagan, and S.J. Livingston. "Hydrologic and erosion calculations in the Water Erosion Prediction Project (WEPP) watershed model." *American Society of Agricultural and Biological Engineers*, 1994: No. 94-2037.

4. Batjes, N. H. "Total Carbon and Nitrogen in the Soils of the World." *European Journal of Soil Science* 47, no. 2 (1996): 151-63.

5. Blake, G. R., and K.H. Hartge, Bulk density, In: Klute, A. (Ed.), *Methods of soil analysis: Part I. Physical and mineralogical methods*, Soil Science Society of America, Agronomy, Monologue 9, no. 2 (1986): 363-375.

6. Bolstad, P. *GIS Fundamentals - A First on Geographic Information Systems, 3rd Ed.*, White Bear Lake, Minnesota: AtlasBooks, 2008.

7. Bosch, D. D., and C. A. Onstad. "Surface Seal Hydraulic Conductivity as Affected by Rainfall." *Transactions of the Asae* 31, no. 4 (1988): 1120-27.

8. Brakensiek, D.L., W.J. Rawls, and G.R. Stephenson. "Modifying SCS hydrologic soil groups and curve numbers for rengeland soils." *American Society of Agricultural and Biological Engineers*, 1984: PNR-84-203.

9. Burras, C.L., J.M. McLaughlin, S.A. Wills, M. Barker, and E.C. Brummer. *Soil carbon and quality in Seymour and Clarinda soil map units, Chariton Valley, Iowa, Final Report.* ISU Project 400-41-71-4216, 64 pages, Ames, IA: Chariton Valley RC&D, 2005.

10. Campbell, G.S., and S. Shiozawa. "Prediction of hydraulic properties of soils using particle-size distribution and bulk density data." *van Genuchten, M. Th., et al. (ed):Proceedings of the International Workshop on Indirect Method for Estimation Hydraulic Properties of Unsaturated Soils.* Riverside, CA: University of California, 1994. 317-328.

11. Carsel, R. F., and R. S. Parrish. "Developing Joint Probability-Distributions of Soil-Water Retention Characteristics." *Water Resources Research* 24, no. 5 (1988): 755-69.

12. Cosby, B. J., G. M. Hornberger, R. B. Clapp, and T. R. Ginn. "A Statistical Exploration of the Relationships of Soil-Moisture Characteristics to the Physical-Properties of Soils." *Water Resources Research* 20, no. 6 (1984): 682-690.

13. Coulthard, T. J., M. G. Macklin, and M. J. Kirkby. "A Cellular Model of Holocene Upland River Basin and Alluvial Fan Evolution." *Earth Surface Processes and Landforms* 27, no. 3 (2002): 269-288.

14. Dane, J.H., and Mackline M.G. "Field soil hydraulic properties based on physical and mineralogical information." *W Genuchten at al. (red): Proceedings of the International Workshop on Indirect Method for Estimation Hydraulic Properties of Unsaturated Soils.* Riverside, CA: University of California, 1994. 389-403.

15. Diiwu, J. Y., R. P. Rudra, W. T. Dickinson, and G. J. Wall. "Effect of Tillage on the Spatial Variability of Soil Water Properties." *Canadian Agricultural Engineering* 40, no. 1 (1998): 1-8.

16. Downer, C.W., and F.L. Ogden. *GSSHA User's Manual: Gridded Surface Subsurface Hydrologic Analysis, Version 1.43 for WMS 6.1.* ERDC Technical Report, Vicksburg, Miss.: Engineering Research and Development Center, 2002.

17. Driese, S. G., L. D. McKay, and C. P. Penfield. "Lithologic and Pedogenic Influences on Porosity Distribution and Groundwater Flow in Fractured Sedimentary Saprolite: A New Application of Environmental Sedimentology." *Journal of Sedimentary Research* 71, no. 5 (2001): 843-857.

18. Elhakeem, M., Y. Chang, C.G. Wilson, and A.N. Papanicolaou. "Field measurement of saturated hydraulic conductivity at the hillslope scale under different soil series and management practices." *AGU 2009 Fall Meeting, December 14-18, 2009.* San Francisco, California, 2009. Poster.

19. Elhakeem, M., and A. N. Papanicolaou. "Estimation of the Runoff Curve Number Via Direct Rainfall Simulator Measurements in the State of Iowa, Usa." *Water Resources Management* 23, no. 12 (2009): 2455-2473.

20. Eigel, J.D., and I.D. Moore. "Effect of rainfall energy on infiltration into a bare soil." *Proc. of ASAE conference on Advances in Infiltration.* Chicago, IL, 1983. 188-199.

21. Flanagan, D.C., and S.J. Livingston. *USDA-Water Erosion Prediction Project (WEPP).* Technical Documentation, West Lafayette, IN: National Soil Erosion Research Laboratory, USDA-ARS-MWA, 1995.

22. Flanagan, D.C., J.C. Ascough, A.D. Nicks, M.A. Nearing, and J.M. Laflen. "Chapter 1: Overview of the WEPP erosion prediction mode." In *Flanagan, D.C., and Nearing, M.A. (eds.) USDA Water Erosion Prediction Project: Hillslope profile and watershed model documentation. NSERL Reaport No. 10*. USDA-ARS National Soil Erosion Research Laboratory, 1995.

23. Govindaraju, R.S., J.K. Koelliker, A.P. Schwab, and M.K. Banks. "Spatial variability of surface infiltration properties over two fields in the Konza Prairie." *Hzazrdous Waste Research Conference.* Manhattan, Kansas, 1995. Poster.

24. Green, W. H., and G. A. Ampt. "Studies on Soil Physics Part I - the Flow of Air and Water through Soils." *Journal of Agricultural Science* 4 (1911): 1-24.

25. Gupta, R. K., R. P. Rudra, W. T. Dickinson, N. K. Patni, and G. J. Wall. "Comparison of Saturated Hydraulic Conductivity Measured by Various Field Methods." *Transactions of the Asae* 36, no. 1 (1993): 51-55.

26. Gupta, R.K., R.P. Rudra, and G. Parkin. "Analysis of spatial variability of hydraulic conductivity at field scale." *Canadian Biosystems Engineering 48*, 1996: 55-62.

27. Highland, J.D., and R.I. Dideriksen. *Soil Survey of Iowa County.* USDA-SCS, Iowa, 1967.

28. Hipple, K.W., et al. *Use-Dependent Soil Properties Issue Paper.* Soil Survey Division Leadership Document, 7pp, USDA-NRCS, 2003.

29. Jabro, J. D. "Estimation of Saturated Hydraulic Conductivity of Soils from Particle-Size Distribution and Bulk-Density Data." *Transactions of the Asae* 35, no. 2 (1992): 557-560.

30. Jarvis, N. J. "A Review of Non-Equilibrium Water Flow and Solute Transport in Soil Macropores: Principles, Controlling Factors and Consequences for Water Quality." *European Journal of Soil Science* 58, no. 3 (2007): 523-546.

31. Jaynes, W. F., and J. M. Bigham. "Multiple Cation-Exchange Capacity Measurements on Standard Clays Using a Commercial Mechanical Extractor." *Clays and Clay Minerals* 34, no. 1 (1986): 93-98.

32. Khan, M. J., E. J. Monke, and G. R. Foster. "Mulch Cover and Canopy Effect on Soil Loss." *Transactions of the Asae* 31, no. 3 (1988): 706-711.

33. Konen, M.E. *Human impacts on soils and geomorphic processes on the Des Moines Lobe, Iowa.* Iowa State University PhD dissertation, Ames: Iowa State University, 1999.

34. Kravchenko, A. N., and D. G. Bullock. "Correlation of Corn and Soybean Grain Yield with Topography and Soil Properties." *Agronomy Journal* 92, no. 1 (2000): 75-83.

35. Laij, F.J., W.J. Alves, M.Th. van Genuchten, and J.R. Williams. *Unsaturated Soil Hydraulic Database, UNSODA 1.0 User's Manual. Report EPA/600/R-96/095.* Ada, Oklahoma: US Environmental Protection Agency, 1996.

36. Leenhardt, D., M. Voltz, M. Bornand, and R. Webster. "Evaluating Soil Maps for Prediction of Soil-Water Properties." *European Journal of Soil Science* 45, no. 3 (1994): 293-301.

37. Legros, J.P. *Mapping of the Soil.* Enfield, New Hampshire: Science Publishers, 2006.

38. Lin, H. "Hydropedology: Bridging disciplines, scales, and data." *Vadose Zone Journal 2,* 2003: 1-11.

39. Lin, Y. S., Y. W. Lin, Y. Wang, Y. G. Chen, M. L. Hsu, S. H. Chiang, and Z. S. Chen. "Relationships between Topography and Spatial Variations in Groundwater and Soil Morphology within the Taoyuan-Hukou Tableland, Northwestern Taiwan." *Geomorphology* 90, no. 1-2 (2007): 36-54.

40. Linsley, R.K., M.A. Kohler, and J.L. Paulhus. *Hydrology for Engineers, 3rd Ed.* New York: McGraw-Hill, Inc., 1982.

41. Liszka, T. "An interpolation method for an irregular net of nodes". *International Journal for Numerical Methods in Engineering* 20, no. 9 (1984): 1599–1612

42. Lunn, D. J., A. Thomas, N. Best, and D. Spiegelhalter. "Winbugs - a Bayesian Modelling Framework: Concepts, Structure, and Extensibility." *Statistics and Computing* 10, no. 4 (2000): 325-337.

43. McCuen, R.H. *Hydrologic Analysis and Design, 3rd Ed.* New Jersey: Prentice Hall, 2003.

44. McNeill, J.D. *Electromagnetic terrain conducptivity measurement at low induction numbers.* Technical Note TN-6, Ontario, Canada: Geonics Ltd, 1980.

45. Mallants, D., B. P. Mohanty, A. Vervoort, and J. Feyen. "Spatial Analysis of Saturated Hydraulic Conductivity in a Soil with Macropores." *Soil Technology* 10, no. 2 (1997): 115-131.

46. Mohanty, B. P., M. D. Ankeny, R. Horton, and R. S. Kanwar. "Spatial-Analysis of Hydraulic Conductivity Measured Using Disc Infiltrometers." *Water Resources Research* 30, no. 9 (1994): 2489-2498.

47. Morin, J., R. Keren, Y. Benjamini, M. Benhur, and I. Shainberg. "Water Infiltration as Affected by Soil Crust and Moisture Profile." *Soil Science* 148, no. 1 (1989): 53-59.

48. Nearing, M. A., B. Y. Liu, L. M. Risse, and X. Zhang. "Curve Numbers and Green-Ampt Effective Hydraulic Conductivities." *Water Resources Bulletin* 32, no. 1 (1996): 125-136.

49. Nordt, L., M. Orosz, S. Driese, and J. Tubbs. "Vertisol Carbonate Properties in Relation to Mean Annual Precipitation: Implications for Paleoprecipitation Estimates." *Journal of Geology* 114, no. 4 (2006): 501-510.

50. Onstad, C. A., M. L. Wolfe, C. L. Larson, and D. C. Slack. "Tilled Soil Subsidence During Repeated Wetting." *Transactions of the Asae* 27, no. 3 (1984): 733-736.

51. Papanicolaou, A. N., and O. Abaci. "Upland Erosion Modeling in a Semihumid Environment Via the Water Erosion Prediction Project Model." *Journal of Irrigation and Drainage Engineering-Asce* 134, no. 6 (2008): 796-806.

52. Papanicolaou, A.N., and M. Elhakeem. *First estimation of the runoff curve number in the State of Iowa vis direct rainfall simulator measurements.* Des Moine, Iowa: Iowa NRCS-USDA, 2007.

53. Papanicolaou, A.N., C.L. Burras, M. Elhakeem, and C.G. Wilson. *Phase I: Field and laboratory investigation of infiltration on different geomorphic surfaces in a watershed and under different land uses.* Lincoln, Nebraska: A Report prepared for USDA-National Soil Survey Center, 2008.

54. Papanicolaou, A.N., C.L. Burras, M. Elhakeem, and C.G. Wilson. *Phase II: Hydropedological investigations and training on a benchmark catena: Performance of semi-automated measurements of Ksat, via different sensors and under different hydrologica and land management conditions.* Lincoln, Nebraska: A Report prepared for USDA-National Soil Survey Center, 2009.

55. Papanicolaou, A.N., M. Elhakeem, C.G. Wison, C.L. Burras, and B. Oneal. "Observations of soils at the hillslope scale in the Clear Creek Watershed in Iowa, USA." *Soil Survey Horizons 49,* 2008: 83-86.

56. Patton, J.J., C.L. Burras, M.E. Konen, and N.E Molstad. "An accurate and inexpensive apparatus and method for teaching and measuring stable aggregate content in soils." *Journal of Natural Resources and Life Sciences Education,* 2001: 84-88.

57. Potter, K. N. "Soil Properties Effect on Random Roughness Decay by Rainfall." *Transactions of the Asae* 33, no. 6 (1990): 1889-1892.

58. Prior, J.C. *Landforms of Iowa.* Iowa City, Iowa: Burr Oak Press, 1991.

59. Rahman, S., L. C. Munn, R. Zhang, and G. F. Vance. "Rocky Mountain Forest Soils: Evaluating Spatial Variability Using Conventional Statistics and Geostatistics." *Canadian Journal of Soil Science* 76, no. 4 (1996): 501-507.

60. Rawls, W.J., and D.L. Brakensiek. " Estimation of Soil Water Retention and Hydraulic Properties." In *Unsaturated Flow in Hydrologic Modeling: Theory and Practice,* 275-300. Kluwer Academic Publishers Boston, 1989.

61. Rawls, W.J., and D.L. Brakensiek. "Prediction of Soil Water Properties for Hydrologic Modeling." *Preceedings of Symposium on Watershed Management.* New York: American Society of Civil Engineers, 1985. 293-299.

62. Rawls, W. J., D. L. Brakensiek, J. R. Simanton, and K. D. Kohl. "Development of a Crust Factor for a Green Ampt Model." *Transactions of the Asae* 33, no. 4 (1990): 1224-1228.

63. Refsgaard, J.C., and B. Storm. "MIKE SHE." In *Computer Models of Watershed Hydrology*, by V.P. Singh (Ed.), 806-846. Colorado: Water Resource Publications, 1995.

64. Risse, L. M., B. Y. Liu, and M. A. Nearing. "Using Curve Numbers to Determine Base-Line Values of Green-Ampt Effective Hydraulic Conductivities." *Water Resources Bulletin* 31, no. 1 (1995): 147-158.

65. Roth, C. H. "A Framework Relating Soil Surface Condition to Infiltration and Sediment and Nutrient Mobilization in Grazed Rangelands of Northeastern Queensland, Australia." *Earth Surface Processes and Landforms* 29, no. 9 (2004): 1093-1104.

66. Ruhe, R.V. *Quaternary Landscapes in Iowa.* Ames, Iowa: Iowa State University Press, 1969.

67. Saxton, K. E., W. J. Rawls, J. S. Romberger, and R. I. Papendick. "Estimating Generalized Soil-Water Characteristics from Texture." *Soil Science Society of America Journal* 50, no. 4 (1986): 1031-1036.

68. Schaap, M.G. *Rosetta Version 1.0.* . Riverside, California: U.S. Salinity Laboratory, Agricultural Research Service- USDA, 1999.

69. Schaap, M. G., F. J. Leij, and M. T. van Genuchten. "Neural Network Analysis for Hierarchical Prediction of Soil Hydraulic Properties." *Soil Science Society of America Journal* 62, no. 4 (1998): 847-855.

70. Schoeneberger, P. J., and D. A. Wysocki. "Hydrology of Soils and Deep Regolith: A Nexus between Soil Geography, Ecosystems and Land Management." *Geoderma* 126, no. 1-2 (2005): 117-128.

71. Schulmeister, M. K., J. J. Butler, J. M. Healey, L. Zheng, D. A. Wysocki, and G. W. McCall. "Direct-Push Electrical Conductivity Logging for High-Resolution Hydrostratigraphic Characterization." *Ground Water Monitoring and Remediation* 23, no. 3 (2003): 52-62.

72. Scokaert, P.O.M., D.Q. Mayne, and J.B. Rawlings. "A new look at the statistical model identification." *Ieee Transactions On Automatic Control,* 1974: 716-723.

73. Shahin, M., H.L. van Orschot, and S.J. Delange. *Statistical Analysis in Water Resources Engineering.* Rotterdam, Netherlands: A. A. Balkema, 1993.

74. Simth, R.E. *Infiltration theory for hydrologic Applications.* Washington, DC: American Geophysical Union, 2002.

75. Smith, R. E., D. C. Goodrich, and J. N. Quinton. "Dynamic, Distributed Simulation of Watershed Erosion - the Kineros2 and Eurosem Models." *Journal of Soil and Water Conservation* 50, no. 5 (1995): 517-520.

76. Soil Survey staff. *Keys to soil taxonomy, 8th ed.* Washington, DC: U.S. Government Printing Office, 1998.

77. Soil Survey staff. *Soil Survey Manual, USDA Agricultrual Handbook, No. 18.* Washington, DC: U.S. Government Printing Office, 1993.

78. Tietje, O., and O. Richter. "Stochastic modeling of the unsaturated water flow using autocorrelation spatially variable hydraulic parameters." *Modeling Geo-Biosphere Processes 1(2)*, 1992: 163-183.

79. Tobler, W. R. "Smooth Pycnophylactic Interpolation for Geographical Regions." *Journal of the American Statistical Association* 74, no. 367 (1979): 519-30.

80. Tobler, W.R., U. Deichmann, J. Gottsegen, and K. Maloy. *The Global Demography Project.* Santa Barbara, California: National Centre for Geographic Information and Analysis (NCGIA), University of California Santa Barbara (UCSB), 1995.

81. Tugel, A. J., J. E. Herrick, J. R. Brown, M. J. Mausbach, W. Puckett, and K. Hipple. "Soil Change, Soil Survey, and Natural Resources Decision Making: A Blueprint for Action." *Soil Science Society of America Journal* 69, no. 3 (2005): 738-747.

82. Tugel, A.J., J. Ward, J.E. Herrick, P. Biggam, C. Seybold, M.D. Remmenga, E.C. Benham, B. Bestelmeyer, A. Moore, F. Young, K. Hipple, B. Ypsilantes, R. Davis. "Sampling dynamic soil properties and vegetation for soil survey and ecological site descriptions." *SRM 60th Annual Meetings, Reno, NV. February 10-15, 2007*. (CD ROM) SRM, Lakewood, CO, 2007.

83. USDA-NRCS. *Hyghway Guide of Iowa Soil Associations.* Des Moines: NRCS, 2008a.

84. USDA-NRCS. "Land resource regions and major land recource areas of the United States, the Caribbean, and the Pacific Basin." *NRCS Major Land Resource Areas Explorer Custom Report.* 2008a. http://www.cei.psu.edu/mlra/ (accessed July 31, 2008).

85. Vereecken, H., J. Maes, and J. Feyen. "Estimating Unsaturated Hydraulic Conductivity from Easily Measured Soil Properties." *Soil Science* 149, no. 1 (1990): 1-12.

86. USDA-NRCS. *Web Soil Survey.* 2008. http://websoilsurvey.nrcs.usda.gov/app/ (accessed July 31, 2008).

87. Vieux, B.E. *Distributed Hydrologic Modeling Using GIS.* New York: Springer-Verlag New York Inc., 2004.

88. Webster, R., and M.A. Oliver. *Geostatistics for Environmental Scientists.* London, United Kingdom: John Wiley and Sons, 2001.

89. West, L.T., M.A. Abreu, and J.P. Bishop. "Saturated hydraulic conductivity of soils in the Southern Piedmont of Georgia, USA: Field evaluation and relation to horizon and landscape properties." *Catena 73*, 2008: 174-179.

90. Witten, T. A., and L. M. Sander. "Diffusion-Limited Aggregation, a Kinetic Critical Phenomenon." *Physical Review Letters* 47, no. 19 (1981): 1400-1403.

91. Wosten, J. H. M., A. Lilly, A. Nemes, and C. Le Bas. "Development and Use of a Database of Hydraulic Properties of European Soils." *Geoderma* 90, no. 3-4 (1999): 169-185.

92. Wu, L., L. Pan, J. Mitchell, and B. Sanden. “Measuring saturated hydraulic conductivity using a generalized solution for single-ring infiltrometers.” *Soil Science Society of America Journal* 63 (1999): 788-792.

93. Zaslavsky, D., and G. Sinai. "Surface Hydrology: IV-Flow in Sloping, Layered Soil." *Journal of the Hydraulics Division 107*, 1981: 53-64.

APPENDIX A. K_{sat} MEASUREMENTS

Table A1. K_b measurements via the Double Ring Infiltrometer

Location	Summer		Fall	
	K_b (mm/hr)	Time (hr)	K_b (mm/hr)	Time (hr)
CRP-1	2.00	6.2	2.60	5.2
CRP-2	7.30	1.9	6.80	1.9
CRP-3	10.50	0.5	9.70	0.5
CRP-4	0.90	13.8	1.20	16.1
CRP-5	6.73	1.8	7.50	1.9
CRP-6	13.43	0.6	12.10	0.5
CRP-7	0.55	22.1	0.63	20.1
CRP-8	5.60	1.8	7.50	2.2
CRP-9	7.50	2.9	8.50	1.5
CRP-10	4.50	1.1	5.30	0.8
CT-1	9.20	1.6	5.30	1.5
CT-2	4.12	5.8	2.92	4.9
CT-3	5.60	2.1	5.90	2.5
CT-4	8.25	2.9	5.30	2.5
CT-5	2.95	5.6	3.27	6.2
CT-6	0.66	28.5	0.74	24.1
CT-7	8.78	0.5	9.80	0.9
CT-8	2.50	5.2	1.90	6.9
CT-9	6.50	1.8	5.50	2.1
CT-10	1.00	14.0	0.80	15.0
NT1-1	0.61	25.3	0.52	27.9
NT1-2	5.11	1.6	5.89	1.8
NT1-3	6.30	1.9	6.81	1.5
NT1-4	7.56	1.8	6.98	2.6
NT1-5	10.02	0.7	11.50	0.7
NT1-6	7.82	0.6	7.50	0.5
NT1-7	1.28	11.8	1.10	14.9
NT1-8	4.28	3.1	3.65	4.9
NT1-9	7.70	2.8	6.90	3.5
NT1-10	5.02	1.8	4.80	1.6

Table A2. K_e measurements via the rainfall simulator.

Field	Location	Summer		Fall	
		K_e (mm/hr)	Time (hr)	K_e (mm/hr)	Time (hr)
CRP	Shoulder	4.5	1.2	5.9	0.7
	Back slope	6.5	0.7	5.2	0.6
	Toe slope	2.9	3.1	3.2	2.8
CT-soybean	Shoulder	4.9	1.5	4.2	1.9
	Back slope	6.9	0.8	8.2	0.5
	Toe slope	3.7	2.4	4.1	1.8
NT-soybean	Shoulder	3.4	2.9	4.1	1.6
	Back slope	4.9	1.5	5.2	1.7
	Toe slope	3.3	3.4	5.6	0.5

APPENDIX B. ROSETTA AND WEPP DESCRIPTION

Rosetta is a program developed for estimating soil hydraulic properties from surrogate soil data utilizing hierarchical PTFs (Schaap et al., 2001). Rosetta can estimate water retention parameters, as well as unsaturated and saturated hydraulic conductivity. These parameters are determined using PTFs with various orders of complexity that incorporate sand, silt, and clay percentages, as well as bulk density and water retention points.

WEPP is a physically based, distributed, watershed model that predicts surface runoff and erosion from agricultural fields under different land uses and management practices (Gregory 1982; Alberts et al. 1988; Ascough et al., 1994). The hydrology component of the model is based on Hortonian flow, calculated from a kinematic wave model, and infiltration, calculated by the Green-Ampt Mein-Larson (GAML) model (Flanagan et al., 1995). WEPP can simulate the hydrologic and erosion processes for different hillslopes in a watershed using both single and continuous storm events (Nearing et al., 1996).

The following supplementary equations of WEPP were used to calculate K_{br}.

$$C = -0.0028 + 0.0113(Sa) + 0.125\left(\frac{Cl}{CEC}\right) \tag{B.1}$$

$$CF = \frac{SC}{\left(1 + \frac{\Psi}{100L}\right)} \tag{B.2}$$

$$SC = 0.736 + 0.19Sa \tag{B.3}$$

$$\Psi = 45.119 - 46.68 \times SC \tag{B.4}$$

$$L = 0.147 - 0.15(Sa)^2 - 0.0003(Cl)(BD) \tag{B.5}$$

where, C is soil stability factor (m^2/J), Sa and Cl are the sand and clay contents, respectively, CEC is the cation exchange capacity (meq/100g), CF is the crust factor, SC is the correction factor for partial saturation of the sub-crust soil, Ψ is the steady state capillary potential at the crust/sub-crust interface, L is the wetted depth (m), and BD is the bulk density (kg/m^3).

The following supplementary equations and tables of WEPP were used to calculate K_e.

$$C_{CE} = C_C \cdot C_{CF} \tag{B.6}$$

$$C_{CF} = e^{\left(-0.33\frac{H}{2}\right)} \tag{BI.7}$$

$$C_{RE} = C_{RF} + C_{RS} \tag{B.8}$$

$$C_{RF} = 1 - e^{-cf \cdot M_f} \tag{B.9}$$

where C_{CE} is the effective canopy cover, C_C is the canopy cover that ranges from 0 to 1, C_{CF} is the correction factor of effective canopy cover, H is the fall height or canopy height (m), C_{RE} is the effective residue cover, C_{RF} is the flat residue cover, C_{RS} is the standing residue cover, M_f is the flat residue biomass which is calculated from the WEPP model, and cf is the crop specific constant that is specified by the type of crops (m^2/kg). The following table provides the values of cf for this study:

Table B1. Parameter values used in the cropland residue decomposition submodel.

Symbol		*cf*	*H*
Variable		CF	CUTHGT
Crop	Fragility Group	$(m^2 \cdot kg^{-1})$	*(m)*
Alfalfa	Non-Fragile	5.0	0.152
Bromegrass	Non-Fragile	5.0	0.152
Canola	Fragile	5.0	0.152
Corn	Non-Fragile	2.1	0.304
Cotton	Non-Fragile	1.9	0.900
Oats	Non-Fragile	5.1	0.152
Peanut	Fragile	2.1	0.100
Ryegrass	Non-Fragile	4.0	0.152
Sorghum	Non-Fragile	2.9	0.609
Soybeans	Fragile	5.2	0.152
Tobacco	Non-Fragile	2.5	0.000
Wheat; Spring	Non-Fragile	6.4	0.152
Wheat; Winter	Non-Fragile	6.4	0.152

Source: WEPP User Summary, USDA-ARS, 1995.

APPENDIX C. FORTRAN CODES FOR TRANSFORMING THE USDA-NRCE PEDON

CODE I.

```
PROGRAM SOIL_DATA_READER
IMPLICIT NONE

CHARACTER*40 INPUT,OUTPUT

INTEGER:: M,HN
CHARACTER*20 A
CHARACTER*20 B(100),C(100),D(100),E(100),F(100),G(100),H(100),I(100)
REAL:: CLAY(100),SILT(100),SAND(100),BULK(100),J(100)

WRITE(*,*)"INPUT FILE NAME"
READ(*,*)INPUT
WRITE(*,*)"OUTPUT FILE NAME"
READ(*,*)OUTPUT

OPEN(UNIT=10, FILE=INPUT)
OPEN(UNIT=11, FILE=OUTPUT)

WRITE(11,'(1X,A8,1X,A4,2X,A4,2X,A4,2X,A6)')'HORIZONS','SAND','SILT','CLAY','BULK-D'

49   READ(10,'(A4)')A
  IF (A .EQ. 'PSDA') THEN
     DO M=1,6
        READ(10,*)B(M)
     END DO
     DO M=1,20
     READ(10,*,ERR=51)B(M),C(M),D(M),E(M),CLAY(M),SILT(M),SAND(M)
     HN=M
     END DO

51    READ(10,'(A4)')A
     IF (A .EQ. 'Bulk') THEN
        DO M=1,5
           READ(10,*)B(M)
        END DO

        DO M=1,20
        READ(10,*,ERR=52)F(M),G(M),H(M),I(M),BULK(M)
         IF (BULK(M) .GT. 2.0) THEN
           BULK(M)=0.0
        END IF
        END DO
     END IF
     GOTO 51
  52   WRITE(11,*)"------", HN
  DO M=1,HN
                        J(M)=SAND(M)+SILT(M)+CLAY(M)
                        IF (J(M) .EQ. 100.0) THEN
     WRITE(11,'(1X,A7,3F6.1,F6.2)')D(M),SAND(M),SILT(M),CLAY(M),BULK(M)
           END IF
           END DO
  END IF
GOTO 49

STOP
END
```

CODE II.

```
PROGRAM HORIZON_A
IMPLICIT NONE

CHARACTER*40 INPUT,OUTPUT
INTEGER::J,K
CHARACTER*8 F,G,H,I
REAL::CLAY,SILT,SAND,BULK,E

WRITE(*,*)"INPUT FILE NAME"
READ(*,*)INPUT
WRITE(*,*)"OUTPUT FILE NAME"
READ(*,*)OUTPUT

OPEN(UNIT=11, FILE=INPUT)
OPEN(UNIT=12, FILE=OUTPUT)

WRITE(*,*)"THE READING TIMES="
READ(*,*)K

DO J=1,K-1
        READ(11,'(A1,A1,A1,A5,3F6.1,F6.2)',ERR=50)F,G,H,I,SAND,SILT,CLAY,BULK
        IF ((G .EQ. '-') .AND. (J .NE. 2)) THEN
                WRITE(12,'(1X,A10)')'PADON MARK'
        END IF

        IF (G .EQ. 'A') THEN
                WRITE(12,'(3F6.1,F6.2)')SAND,SILT,CLAY,BULK
        ELSE IF (H .EQ. 'A') THEN
                WRITE(12,'(3F6.1,F6.2)')SAND,SILT,CLAY,BULK
        END IF
50 END DO

E=123.45
WRITE(12,'(F6.2)')E

STOP
END
```

CODE III.

```
PROGRAM HORIZON_B
IMPLICIT NONE

CHARACTER*40 INPUT,OUTPUT
INTEGER::J,K
CHARACTER*8 F,G,H,I
REAL::CLAY,SILT,SAND,BULK,E

WRITE(*,*)"INPUT FILE NAME"
READ(*,*)INPUT
WRITE(*,*)"OUTPUT FILE NAME"
READ(*,*)OUTPUT

OPEN(UNIT=11, FILE=INPUT)
OPEN(UNIT=12, FILE=OUTPUT)

WRITE(*,*)"THE READING TIMES="
READ(*,*)K

DO J=1,K-1
        READ(11,'(A1,A1,A1,A5,3F6.1,F6.2)',ERR=50)F,G,H,I,SAND,SILT,CLAY,BULK
        IF ((G .EQ. '-') .AND. (J .NE. 2)) THEN
                WRITE(12,'(1X,A10)')'PADON MARK'
        END IF

        IF (G .EQ. 'B') THEN
                WRITE(12,'(3F6.1,F6.2)')SAND,SILT,CLAY,BULK
        ELSE IF ((H .EQ. 'B') .AND. (G .NE. 'A')) THEN
                WRITE(12,'(3F6.1F6.2)')SAND,SILT,CLAY,BULK
        END IF
50 END DO

E=123.45
WRITE(12,'(F6.2)')E

STOP
END
```

CODE IV.

```
PROGRAM AVERAGE_CALCULATOR
IMPLICIT NONE

CHARACTER*40 INPUT,OUTPUT
INTEGER::N,LN,L,PEDON
REAL::SAND(100),SILT(100),CLAY(100),BD(100)
REAL::TOTALSA(100),TOTALSI(100),TOTALCL(100),TOTALBD(100)
REAL::AVERSA(100),AVERSI(100),AVERCL(100),AVERBD(100)
REAL::TH33,TH1500

WRITE(*,*)"INPUT FILE NAME:"
READ(*,*)INPUT
WRITE(*,*)"OUTPUT FILE NAME:"
READ(*,*)OUTPUT
WRITE(*,*)"FIRST PEDON NO.="
READ(*,*)PEDON
OPEN(10,FILE=INPUT)
OPEN(11,FILE=OUTPUT)

WRITE(11,'(A49)')'Code Description Sand Silt Clay Bulkd Th33 Th1500'
WRITE(11,'(A44)')'IOWA FIELD DATA % % % gr/cm3 cm3/cm3 cm3/cm3'

TOTALSA(0)=0
TOTALSI(0)=0
TOTALCL(0)=0
TOTALBD(0)=0
PEDON=PEDON-1
TH33=0.00
TH1500=0.00

99                  DO L=1,10
                        READ(10,'(3F6.1,F6.2)',ERR=101)SAND(L),SILT(L),CLAY(L),BD(L)
                        LN=L
                        TOTALSA(L)=SAND(L)+TOTALSA(L-1)
                        TOTALSI(L)=SILT(L)+TOTALSI(L-1)
                        TOTALCL(L)=CLAY(L)+TOTALCL(L-1)
                        TOTALBD(L)=BD(L)+TOTALBD(L-1)
                        IF (SAND(L) .GT. 100) THEN
                        GOTO 103
                        END IF
          100       END DO
          101       AVERSA(N)=TOTALSA(LN)/LN
          AVERSI(N)=TOTALSI(LN)/LN
          AVERCL(N)=TOTALCL(LN)/LN
          AVERBD(N)=TOTALBD(LN)/LN
          PEDON=PEDON+1

          WRITE(11,'(I5,A12,3F6.1,3F6.2)')PEDON,'IOWA(FIELD)',AVERSA(N),AVERSI(N),AVERCL(N),AVERBD(N),TH33,
TH1500
                    GOTO 99
          103 AVERSA(N)=TOTALSA(L-1)/(LN-1)
          AVERSI(N)=TOTALSI(L-1)/(LN-1)
          AVERCL(N)=TOTALCL(L-1)/(LN-1)
          AVERBD(N)=TOTALBD(L-1)/(LN-1)
          PEDON=PEDON+1
          WRITE(11,'(I5,A12,3F6.1,3F6.2)')PEDON,'IOWA(FIELD)',AVERSA(N),AVERSI(N),AVERCL(N),AVERBD(N),TH33,
TH1500

STOP
END
```

APPENDIX D. RATIOS OF K_{br}, $K_{e\text{-}nr}$, AND K_e TO K_b FOR THE MONTH OF APRIL IN THE CCW, IA.

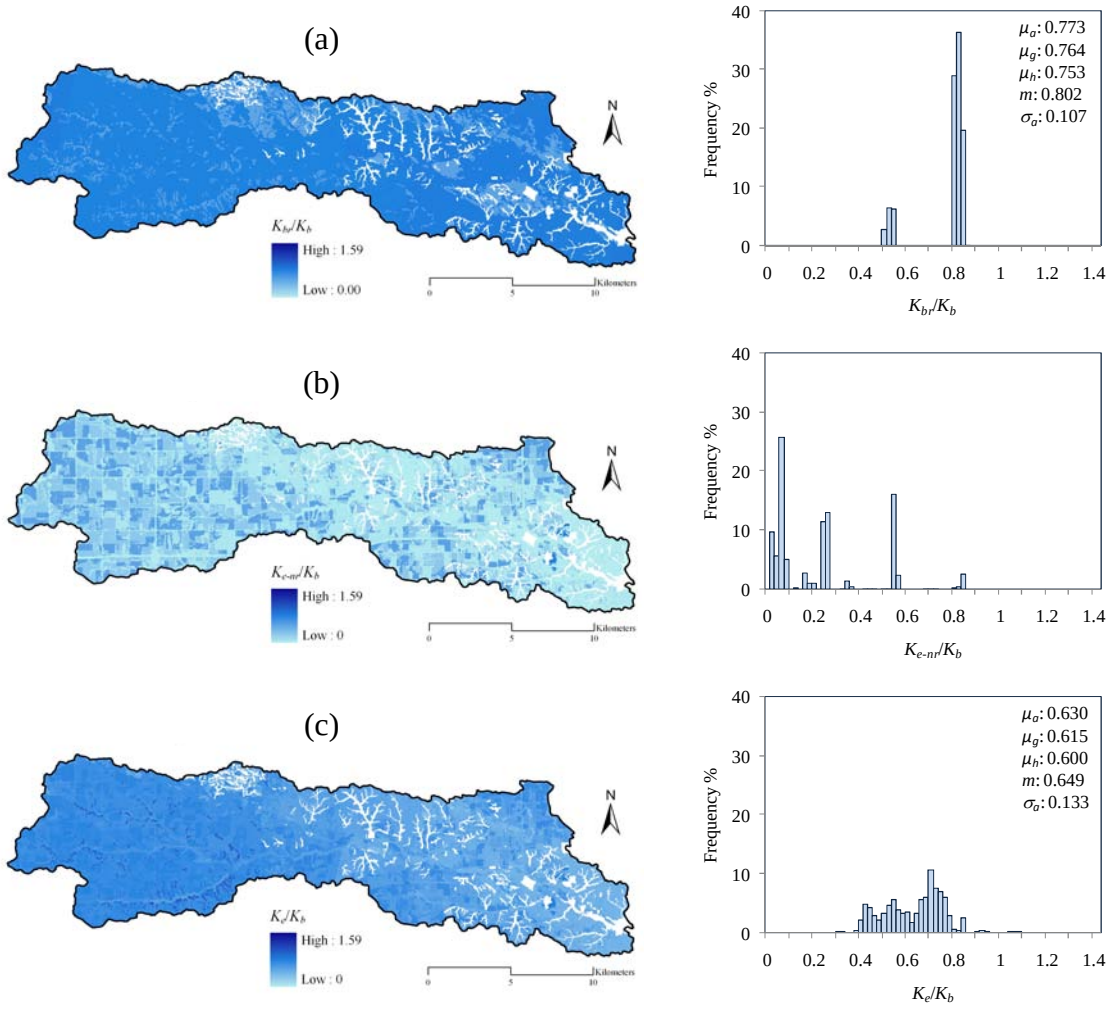

Figure D1. Ratios of K_{br}, $K_{e\text{-}nr}$, and K_e *to* K_b for the month of April in the CCW, IA.